Erschienen in: Inorganic chemistry ; 61 (2022), 32. - S. 12662-12677
https://dx.doi.org/10.1021/acs.inorgchem.2c01608

Reversible Multielectron Release from Redox-Active Three-Dimensional Molecular Barrels with Ruthenium-Alkenyl Moieties

Rajorshi Das,* Michael Linseis, Stefan Scheerer, Katrin Zoller, Laura Senft, Ivana Ivanović-Burmazović, and Rainer F. Winter*

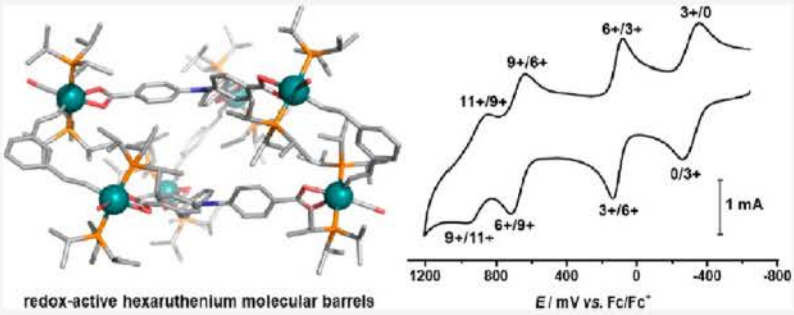

ABSTRACT: Three-dimensional molecular barrels $\mathbf{Ru_6}$-**4** and $\mathbf{Ru_6}$-**5** were synthesized in high yields from dinuclear ruthenium-vinyl clamps and tritopic triphenylamine-derived carboxylate linkers and characterized by multinuclear NMR spectroscopy including ^{1}H–^{1}H COSY and ^{1}H DOSY measurements, high-resolution electrospray ionization mass spectrometry, and X-ray crystallography. The metal frameworks of the cages adopt the shape of twisted trigonal prisms, and they crystallize as racemic mixtures of interdigitating Δ- and Λ-enantiomers with a tight columnar packing in $\mathbf{Ru_6}$-**4**. Electrochemical studies and redox titrations revealed that the cages are able to release up to 11 electrons on the voltammetric timescale and that their cage structures persist up to the hexacation level. IR and UV–vis–near-infrared spectroelectrochemical studies confirm substituent-dependent intramolecular electronic communication within the π-conjugated 1,3-divinylphenylene backbone in the tricationic states, where all three divinylphenylene-bridged diruthenium clamps are present in mixed-valent radical cation states. The formation of 1:3 charge-transfer salts with 2,3,5,6-tetrafluoro-7,7,8,8-tetracyanoquinodimethane as the electron acceptor is also demonstrated.

INTRODUCTION

Over the last decades, the bottom-up approach of coordination-driven self-assembly has evolved into the most effective strategy for the rational construction of discrete supramolecular coordination complexes.[1−5] Based on this principle, a large number of structurally diverse polynuclear metallamacrocycles and coordination cages have been realized. Some of them have already found applications in host–guest chemistry,[3,5−7] in gas storage,[8−12] as luminescent materials,[13−24] for charge-transport or as charge-storage systems,[25−28] in catalysis,[21,29−40] and in other fields.[41−43]

Our contributions to this field revolve around utilizing redox-active ruthenium-alkenyl moieties of the type Ru(CO)Cl-(P^iPr_3)$_2$(CH=CHR) or {Ru(CO)Cl(P^iPr_3)$_2$}(μ-CH=CH–arylene–CH=CH) as constituents of tri-, tetra-, or hexaruthenium metallamacrocycles.[44−50] Such compounds may exhibit polyelectrochromism and efficient intramolecular intervalence charge transfer (CT) in their mixed-valent states.[51,52] As an extension of these studies, we now target the synthesis of three-dimensional hexaruthenium cages from the combination of dimetal clamps and tridentate carboxylate linkers. The vast majority of known, discrete hexanuclear supramolecular metallacages were built from planar tridentate ligands as, for example, 2,4,6-tripyridyl-1,3,5-triazine (**TPT**, Figure 1) and diimine-bridged dinuclear complexes of square-planar Pd^{II} or Pt^{II} ions with cis-disposed, substitutionally labile ligands.[2,4,5,7]

Herein, we report the construction of three-dimensional hexaruthenium metallabarrels from *m*-divinylphenylene-bridged diruthenium-alkenyl complexes and triphenylamine-4,4′,4″-tricarboxylate as the tritopic linker in high-yielding self-assembly processes. The twisted, propeller-shaped conformation of the triphenylamine (TPA) core proved to be crucial for the

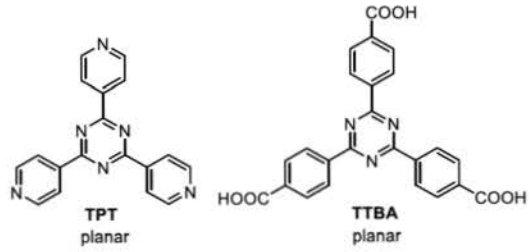

Figure 1. Chemical structures of planar 2,4,6-tripyridyl-1,3,5-triazine (**TPT**, left) and 4,4′,4″-[1,3,5]triazine-2,4,6-triyl-tris(benzoic acid) (**TTBA**, right).

successful formation of discrete cage structures. The resulting hexanuclear cages can release a total of six electrons in two discrete three-electron redox steps without structural disintegration and exhibit strong responses in their electronic spectra as a consequence of electron transfer. We also show that, due to their low oxidation potentials, the present cages form 1:3 CT salts with the strong organic electron-acceptor 2,3,5,6-tetrafluoro-7,7,8,8-tetracyanoquinodimethane (F_4TCNQ).

■ RESULTS AND DISCUSSION

The formation of supramolecular complexes generally relies on reversible metal−ligand bond-forming and -breaking processes, which will ultimately transform initially formed mixtures of mono- and oligonuclear species into discrete metallamacrocyclic or cage structures under thermodynamic control.[53−60] The selective transformations of intermittently formed dicarboxylate-bridged tetra- or hexaruthenium metallamacrocycles into larger octa- or smaller tetraruthenium ones on prolonged warming provide recent examples in ruthenium-alkenyl chemistry that are related to the present work.[45,46,61] Attempts to obtain hexaruthenium cages by reacting the *m*-divinylphenylene-bridged diruthenium clamps **Ru_2-2** or **Ru_2-3** of Scheme 1 with the deprotonated planar[62,63] 1,3,5-trisubstituted triazine-derived linker **TTBA** of Figure 1 were not met by success. To our delight, their reaction with the conformationally more flexible, propeller-shaped triphenylamine-4,4′,4″-tricarboxylate, which was obtained from the deprotonation of the parent tricarboxylic acid **1** with potassium carbonate, at 40 °C in methanol/dichloromethane yielded, after 30 h, hexaruthenium cages **Ru_6-4** or **Ru_6-5** in yields of 90 or 87%.

Metallacages **Ru_6-4** and **Ru_6-5** were characterized by multinuclear NMR spectroscopy and high-resolution electrospray ionization mass spectrometry (HR-ESI MS). Figure 2 displays the ^{1}H NMR spectra in the region of the aryl and alkenyl protons with their integrations and assignments. Additional NMR spectra including the results of ^{1}H−^{1}H correlation spectroscopy (COSY) experiments to support the signal assignments are provided in Figures S1−S12. For example, in the ^{1}H NMR spectra, the alkenyl protons were detected at δ = 8.99 (Ru−C*H*) and 6.25 ppm (Ru−CH=C*H*) (d, $^3J_{H,H}$ = 15.3 Hz) for **Ru_6-4** and at δ = 8.60 and 6.54 ppm (d, $^3J_{H,H}$ = 15.2 Hz) for **Ru_6-5**. The resonances of the corresponding carbon atoms appeared at δ = 160.5 (Ru−CH) and 133.7 ppm (Ru−CH=*C*H) for **Ru_6-4** and at δ = 155.5 and 126.5 ppm for **Ru_6-5** in the ^{13}C{^{1}H} NMR spectra. The carbonyl carbon atoms were observed at δ = 208.9 or at 209.0 ppm for **Ru_6-4** and **Ru_6-5**, respectively, as triplets with a coupling constant $^2J_{P-C}$ of 15.2 Hz. Interestingly, in the ^{31}P{^{1}H} NMR spectra of both molecular cages, two doublet resonances at δ = 37.0 and 39.1 ppm (for

Scheme 1. Synthesis of Three-Dimensional Hexaruthenium Metallabarrels Ru_6-4 and Ru_6-5

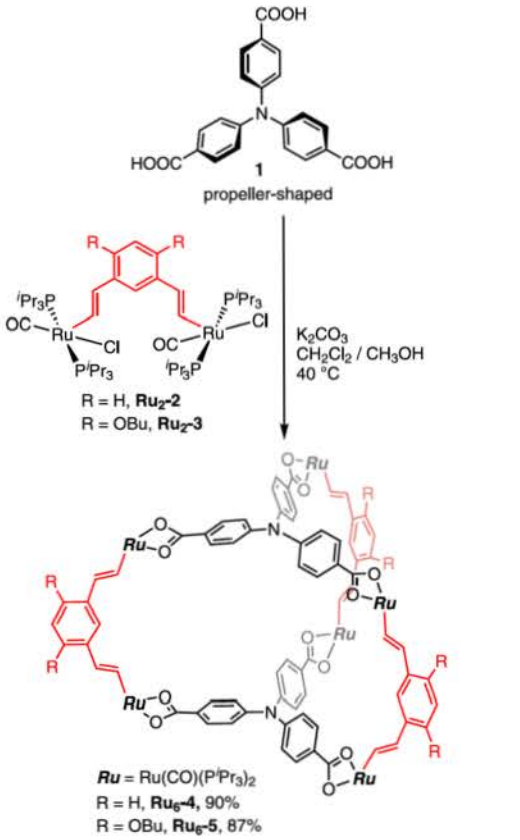

Ru_6-4) and δ = 36.8 and 38.3 ppm (for **Ru_6-5**) with a large $^2J_{P-P}$ coupling constant of 275 Hz were observed, which is typical for mutually trans-disposed phosphine ligands. This indicates that the two P^{i}Pr$_3$ ligands of every ***Ru*** entity (***Ru*** = Ru(CO)(P^{i}Pr$_3$)$_2$) are in different chemical environments, that is, the lack of a mirror plane through the *m*-divinylphenylene bridging ligand.

In line with this observation, aryl protons 9/9′ and 10/10′ at the triphenylamine (TPA) linker gave rise to four separate doublet resonances at δ = 8.09 and 7.95 ppm (H9/9′) and 7.29 and 7.09 ppm (H10/10′) for **Ru_6-4** and δ = 8.05 and 7.95 ppm (H9/9′) and at 7.28 and 7.09 ppm (H10/10′) for **Ru_6-5**, obviously as a result of hindered phenyl rotation. Closer inspection of the room temperature (rt) NMR spectra revealed specific broadening of the latter resonances. This prompted us to record ^{1}H NMR spectra in 5 K steps over a *T* interval of 273 to 303 K, as shown in Figures S11 and S12. Further warming increased the broadening, while cooling had the opposite effect until, at 278 K, the half-widths of the TPA aryl resonances became identical to those of the alkenyl and phenyl protons at the bridging *m*-divinyphenylene ligand. This suggests the onset of a dynamic process at or near rt, which is due to either phenyl ring rotation or a twisting motion of the distorted prismatic cage structure (vide infra). ^{1}H diffusion ordered spectroscopy (DOSY) NMR spectra confirmed that all resonances are due to one defined molecular species in each case with a diffusion coefficient of 7.08×10^{-10} m^2 s^{-1} for **Ru_6-4** and 5.62×10^{-10} m^2 s^{-1} for bulkier **Ru_6-5** (see Figures S5 and S10).

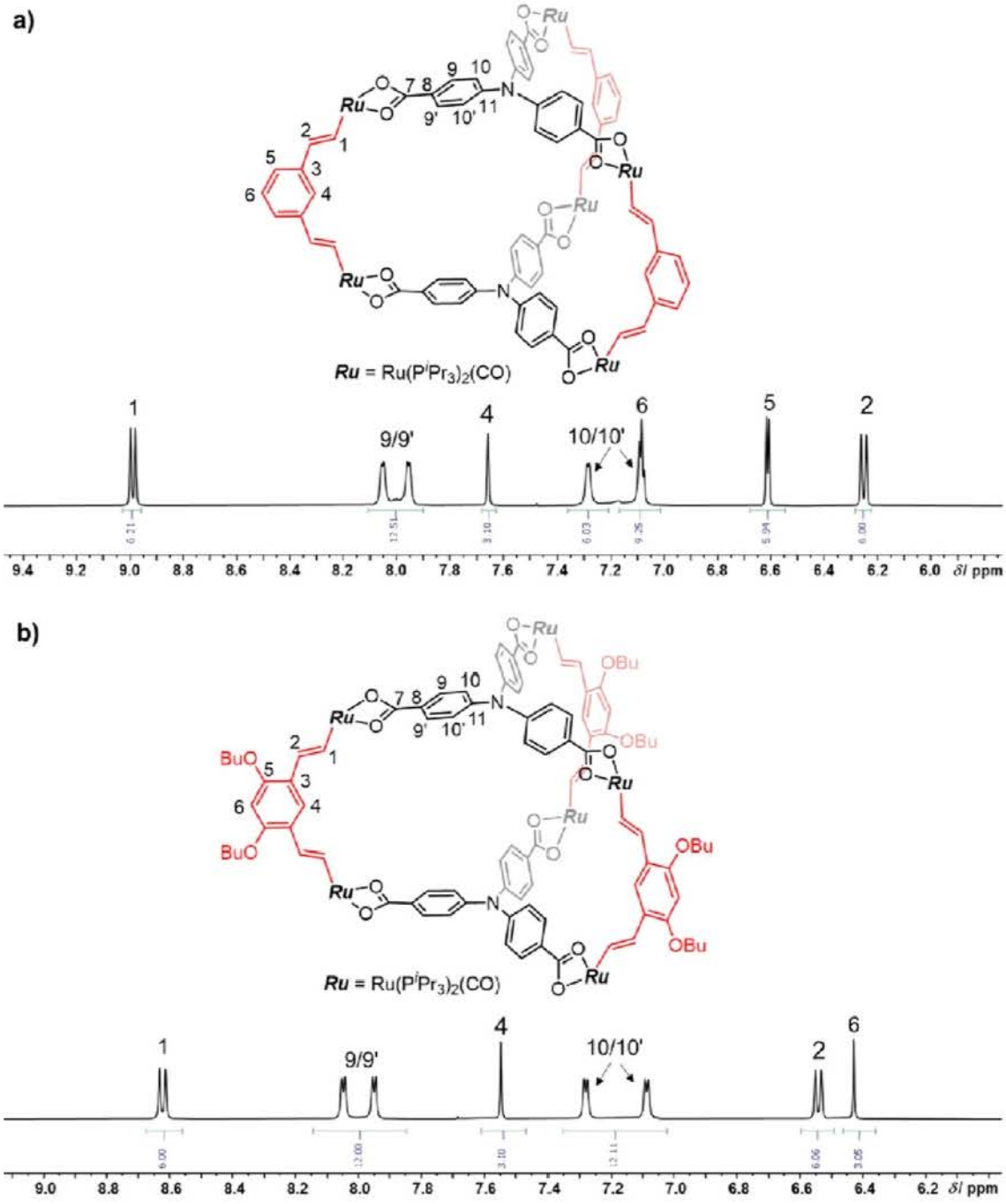

Figure 2. ^{1}H NMR spectra of (a) **Ru$_6$-4** and (b) **Ru$_6$-5** in CD_2Cl_2 at 298 K in the region of aryl and alkenyl protons.

HR-ESI MS confirmed the molecular compositions of the new complexes as the envisioned hexaruthenium species. The mass peak of the molecular ion $[\mathbf{Ru_6\text{-}4}]^{2+}$ was detected at m/z = 1915.6789 (calcd. m/z = 1915.6917 for $C_{186}H_{300}N_2O_{18}P_{12}Ru_6$) with half-integer spacings between individual isotopic peaks. An additional, less intense signal could be assigned to the $[M - H]^+$ ion (m/z = 3830.3612; calcd. m/z = 3830.3754 for $C_{186}H_{299}N_2O_{18}P_{12}Ru_6$). In the case of **Ru$_6$-5**, the most intense peak was that of the molecular dication $[\mathbf{Ru_6\text{-}5}]^{2+}$, which appeared at m/z = 2131.8525 (calcd. m/z = 2131.8647 for $C_{210}H_{348}N_2O_{24}P_{12}Ru_6$). The observed isotopic patterns match with the calculated ones (Figure 3; see also Figure S13). The molecular ion peak for the corresponding trication $[\mathbf{Ru_6\text{-}5}]^{3+}$ was observed at m/z = 1421.2332 (calcd. 1421.2430 for $C_{210}H_{348}N_2O_{24}P_{12}Ru_6$) with spacings of 0.33 amu between neighboring peaks within the isotopic envelope.

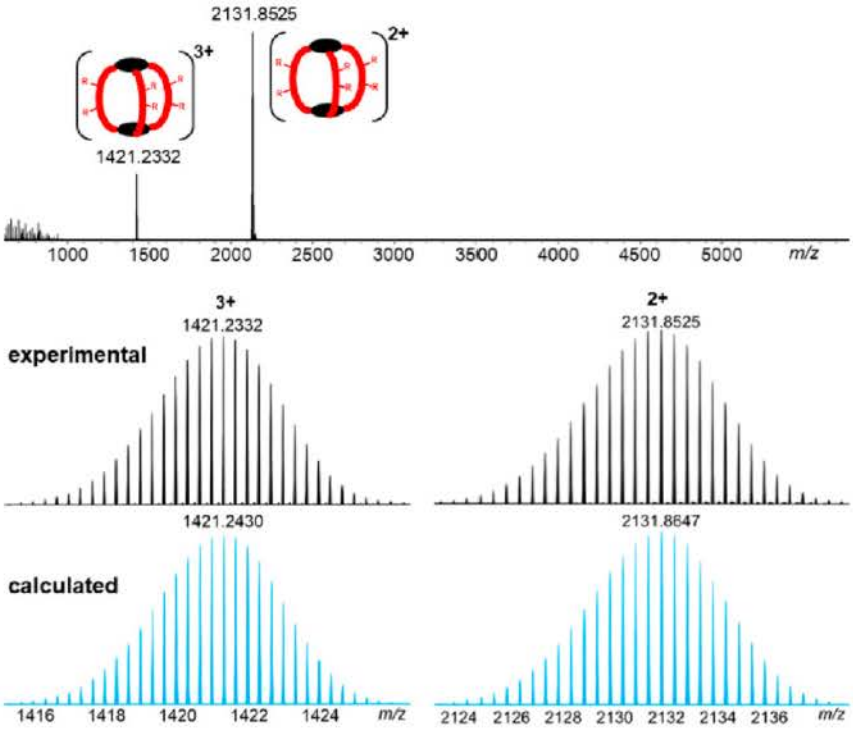

Figure 3. HR-ESI (positive ion mode) mass spectrum of **Ru_6-5** (R = OBu). Full scale (top) and comparison of isotopic distributions (bottom) for the di- and tricationic species of the experimental spectrum (black lines) with the calculated ones (blue lines).

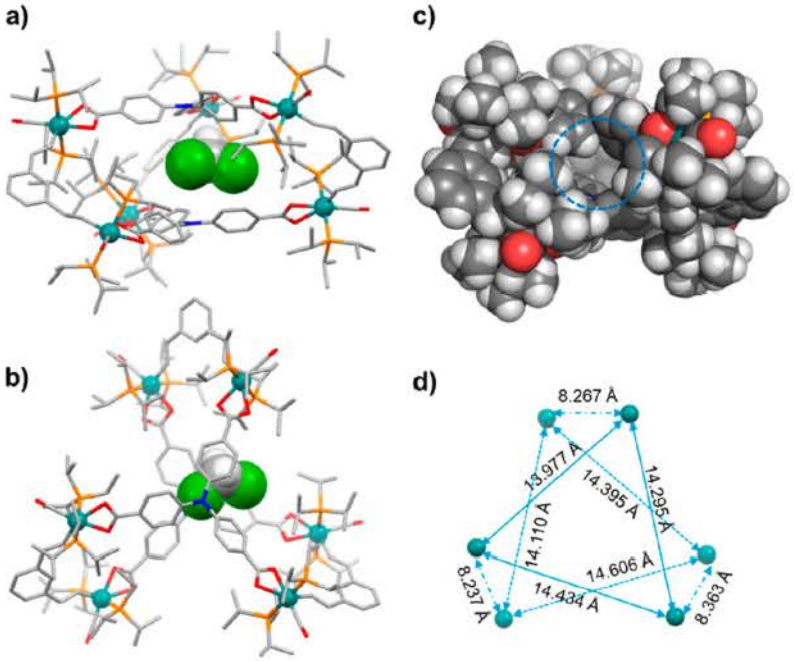

Figure 4. X-ray structure of **Ru_6-4** in **Ru_6-4**·5CH_2Cl_2·CH_3OH. Solvent molecules and hydrogen atoms, except for one CH_2Cl_2 molecule which is trapped in between the two triphenylamine linkers via strong CH···π interactions, are removed for clarity reasons. (a) Side view and (b) top view of the barrel-like molecule **Ru_6-4**. (c) Space-filling model showing the cavity inside the molecular barrel. (d) Ru···Ru distances within the Ru_3-TPA triangles and the divinylphenylene straps of the twisted trigonal Ru_6 prism. Color codes: gray, carbon; red, oxygen; orange, phosphorus; white, hydrogen; green, chlorine; dark turquoise, ruthenium.

The identities and structures of cage compounds **Ru_6-4** and **Ru_6-5** were finally established by X-ray diffraction analysis on single crystals of **Ru_6-4**·$5CH_2Cl_2$·CH_3OH and of **Ru_6-5**·$2CH_2Cl_2$ that were grown by layering a methanolic solution of the TPA tricarboxylate ligand on a dichloromethane solution of diruthenium complex **Ru_2-2** or **Ru_2-3**. **Ru_6-4** crystallized in the triclinic space group $P\bar{1}$, whereas two different polymorphs were found for complex **Ru_6-5**, one with a hexagonal (space group $R\bar{3}$) and one with a triclinic unit cell. Both were suitable for X-ray crystallography but suffered from various difficulties. The specimen with the space group $R\bar{3}$ disintegrated within 8 days on the diffractometer, so that only an incomplete data set (76% completeness) could be obtained; this however refined well. Several other crystals we picked had all crystallized in the triclinic crystal system, were twinned, and suffered from severe disorder of the butoxy and P^iPr_3 groups during refinement. The structure of **Ru_6-4** is shown in Figures 4 and S14 and S15, while that of **Ru_6-5** in the space group $R\bar{3}$ is shown in Figure S16. Figures 5 and S17 illustrate the packing of individual cage molecules in the crystal lattice. Tables S1–S4 provide the crystallographic details.

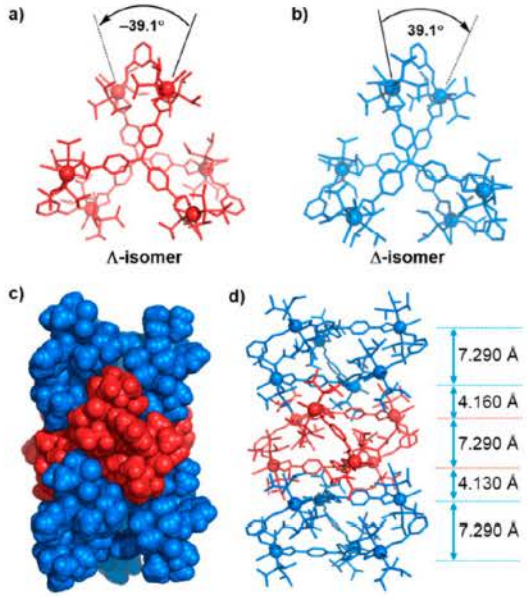

Figure 5. (a,b) Top views of Λ- and Δ-enantiomers present in the unit cell of **Ru_6-4**. (c) One-dimensional columnar structure formed by alternating Λ- and Δ-isomers. (d) Ball and stick representation with intermolecular N···N distances along the stacking axis.

Both cages adopt the shape of a twisted trigonal prism. Steric repulsion between the ortho protons tilts adjacent phenyl rings of the tritopic TPA linkers from planarity, giving them their usual propeller structures. This rotation may provide the necessary conformational freedom to forge two TPA linkers and three *m*-divinylphenylene diruthenium complexes into discrete three-dimensional molecular cage structures. Due to the twisted conformations of the diruthenium clips, one of the two P^iPr_3 ligands at every ruthenium ion points to the outside of the barrel-like structure, whereas the other one is more poised toward its interior, which is in line with the observation of two sets of chemically and magnetically distinct P^iPr_3 ligands in NMR spectroscopy. The two triangular planes spanned by the nitrogen atoms of the triphenylamine-4,4′,4″-tricarboxylate linkers and the immediately attached *ipso* carbon atoms of the phenyl residues are separated by 7.290 Å for **Ru_6-4** and 7.924 Å for **Ru_6-5** (Figures 4b and 5a,b). The Ru···Ru distances at the TPA-bridged triangles of **Ru_6-4** measure 13.977 to 14.606 Å, while those at the divinylarylene straps are shorter and range from 8.237 to 8.363 Å (Figure 4d). The corresponding dimensions of the **Ru_6-5** cage are 14.288 and 8.326 Å, respectively. The Ru−P, Ru−C_{CO}, and Ru−$C_{alkenyl}$ bond lengths fall in the range of 2.390(3) to 2.444(2), 1.753(9) to 1.819(10), and 1.964(9) to 2.006(8) Å, respectively. The P−Ru−P bond angles of the trans-disposed P^iPr_3 ligands measure 175.79(8) to 177.14(8); they comply with those for macrocyclic complexes with six-coordinated Ru-alkenyl complexes of the type Ru(CO)Cl(P^iPr_3)$_2$(CH=CHR)(κ^2O,O'-OOCR′).[44,46,47,50]

Notably, the unit cell of complex **Ru_6-4** contains a pair of tightly packed, interdigitating molecules with a rather close separation of 4.160 Å between the TPA N atoms. These two molecules represent the Δ- and Λ-enantiomers of a twisted trigonal prism with (anti)clockwise rotations of +39.1° (Δ) or −39.1° (Λ) between the two TPA-bridged triangular faces. Similar to **Ru_6-4**, the unit cell of **Ru_6-5** also contains pairs of enantiomers with twist angles of +36.3° (Δ-isomer) and −36.3° (Λ-isomer, Figure S17). This kind of distortion is reminiscent of snapshots of the interconversion between the Δ- and Λ-isomers of octahedral tris(chelate) complexes according to the Bailar twist. As a consequence of twisting, the ruthenium-vinyl moieties at the *m*-divinylphenylene straps are non-coplanar with angles of 24.8 to 32.6° in **Ru_6-4** and of 36.5° in **Ru_6-5** between the planes of interlinked Ru−CH=CH− entities. Rotations around the ruthenium-alkenyl bonds of such complexes are usually associated with energy barriers of 22 to 31 kJ mol^{-1} and less than 7 kJ·mol^{-1} for a rotation by 40° so that the two enantiomers are expected to interconvert in solution.[64,65]

In the case of **Ru_6-4**, the complementary shapes of the two different enantiomers lead to the formation of tightly packed columnar stacks of alternating ···Λ···Δ··· enantiomers with even shorter N···N separations of 4.130 Å between the molecule pairs of the unit cell. Strong CH···π (2.730–2.899 Å) and CH···$O_{carboxylate}$ ($d_{CH\cdots O}$ = 2.563 to 2.691 Å) interactions exist between adjacent molecules (Figure S14). However, the bulky butoxy groups at the periphery of **Ru_6-5** only allow for the formation of interdigitating dimers with a separation N···N of 4.001 Å and CH···π contacts of 2.618 to 2.795 Å but prevent their further association into a columnar structure comparable to **Ru_6-4**. In both cages, a molecule of dichloromethane is trapped as a guest in between the two TPA linkers (Figures 4 and S15). Short CH···π interactions with a distance of 2.525 Å between the CH_2Cl_2 molecule and the π-electron cloud of a nearby phenyl ring of one TPA unit are observed in **Ru_6-4**.

As mentioned in the outline, the divinylphenylene-diruthenium building blocks are redox-active and are capable of undergoing two sequential one-electron oxidations per diruthenium constituent.[66] Metallamacrocycles, where two or three such entities are clamped by insulating dicarboxylate linkers, show doubling or tripling of the number of electrons transferred in each step, sometimes with small potential splittings for a composite wave that represents the stepwise charging of the divinylarylene diruthenium constituents.[45,47–49] Similar observations were reported for a variety of other metallamacrocycles and cages that contain identical redox-active constituents.[16,67–75] The TPA linkers are likewise redox-active,

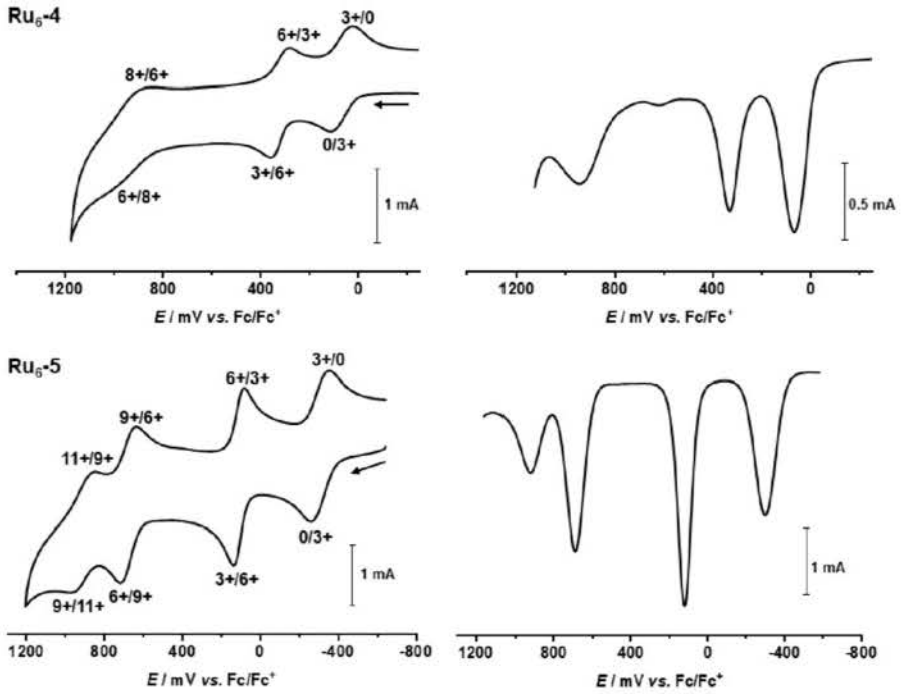

Figure 6. Cyclic voltammograms of $\mathbf{Ru_6}$**-4** and $\mathbf{Ru_6}$**-5** (CH_2Cl_2/0.1 M NBu_4^+ PF_6^-, 295(±3) K, scan rate ν = 100 mV s^{-1}). Potentials are referenced to the FcH/FcH^+ redox couple.

Table 1. Cyclic Voltammetry Data of $\mathbf{Ru_6}$-4 and $\mathbf{Ru_6}$-5[a]

	$E_{1/2}^{0/3+}(\Delta E_p)$ or $[E_{1/2}^{0/+}]$	$E_{1/2}^{3+/6+}(\Delta E_p)$ or $[E_{1/2}^{+/2+}]$	$\Delta E_{1/2}^{3+/6+}$ or $[\Delta E_{1/2}^{+/2+}]$	$E_{1/2}^{6+/8+}(\Delta E_p)$ or $[E_{1/2}^{6+/9+}(\Delta E_p)]$	$\Delta E_{1/2}^{6+/8+}$ or $[\Delta E_{1/2}^{6+/9+}]$	$E_{1/2}^{9+/11+}(\Delta E_p)$	$\Delta E_{1/2}^{9+/11+}$
$\mathbf{Ru_2}$**-2**	[190]	[460]	[270]	n. a.	n. a.	n. a.	n. a
$\mathbf{Ru_2}$**-3**	[−200]	[225]	[425]	n. a.	n. a.	n. a	n. a
$\mathbf{Ru_6}$**-4**	70 (105)	320 (75)	250	925 (196)	605	n. a.	n. a.
$\mathbf{Ru_6}$**-5**	−305 (91)	110 (57)	415	[680 (88)]	[565]	930 (138)	250

[a]All data in millivolts versus FcH/FcH^+ in CH_2Cl_2/NBu_4PF_6 at rt and at ν = 100 mV s^{-1}.

and each of them may undergo one-electron oxidation to the corresponding $TPA^{\bullet+}$ radical cation ($E_{1/2}$ of the free acid in CH_3CN = 0.80 V).[76] This endows the present cages with the capability to reversibly release a maximum of 11 electrons. As we will show in the following, up to 6 electrons can be reversibly extracted from these cages without disintegration of their structures.

The electrochemical behavior of the two hexaruthenium cages was first investigated by cyclic voltammetry (CV). Cyclic voltammograms recorded at a sweep rate of 0.1 V·s^{-1} are shown in Figure 6 and pertinent data are collected in Table 1. The chloro-substituted *m*-divinylphenylene-bridged precursor complexes $\{(P^iPr_3)_2Cl(CO)Ru\}_2(\mu\text{-}CH{=}CH{-}C_6H_2R_2{-}CH{=}CH{-})$ $\mathbf{Ru_2}$**-2** (R = H) and $\mathbf{Ru_2}$**-3** (R = OBu, Scheme 1) undergo two stepwise one-electron oxidations at half-wave potentials of 190 and 460 mV or of −200 and 225 mV, respectively, in the CH_2Cl_2/0.1 M NBu_4^+ PF_6^- electrolyte (Table 1).[66,77] Under the same conditions, complex $\mathbf{Ru_6}$**-4** showed three consecutive oxidations at $E_{1/2}$ = 70, 320, and 925 mV. Voltammograms of $\mathbf{Ru_6}$**-5** exhibited even four redox waves. As for their dinuclear precursors, the presence of two electron-donating butoxy groups at every *m*-phenylene linker lowers the oxidation potentials of $\mathbf{Ru_6}$**-5** by up to 375 mV as compared to $\mathbf{Ru_6}$**-4**. The first two oxidations of the diruthenium clamps were hence observed at $E_{1/2}$ = −305 and at 110 mV with an enhanced redox splitting $\Delta E_{1/2}$ of 415 mV (Table 1). As usual, substitution of the two-electron donor chloro ligands by bidentate, four-electron donor carboxylate ligands lowers the oxidation potentials by more than 100 mV.

Comparison of precursor complexes $\mathbf{Ru_2}$**-2** and $\mathbf{Ru_2}$**-3** and metallamacrocyclic complexes with two or three divinylarylene constituents suggests that the first two waves involve the first and the second oxidations of the three *m*-divinylphenylene-diruthenium entities with the release of a total of six electrons, three in each individual step. This supposition was later confirmed by redox titrations and by monitoring the spectroscopic changes in the UV−vis−near-infrared (NIR) and electron paramagnetic resonance (EPR) spectra on adding appropriate amounts of a suitable chemical oxidant to solutions of $\mathbf{Ru_6}$**-5**. These experiments will be detailed in a later section. Attempts to establish the number of electrons that are released during the first oxidation of $\mathbf{Ru_6}$**-5** by the method of Fawcett and Baranski,[78] that is, by comparing the slopes of the current i versus $t^{-1/2}$ as obtained from chronoamperometry experiments and the limiting currents i_{limit} from linear sweep voltammetry (LSV) to those of the one-electron standard decamethylferrocene (DMFcH), gave a ratio n_{cage}/n_{DMFcH} of 4.2, which, while too high, still confirms a multielectron character. Under the

assumption that n_{cage} equals 3, chronoamperometry provided a diffusion coefficient D of 4.54×10^{-10} m^2 s^{-1} for **Ru$_6$-5** as calibrated against the DMFcH standard,[79] which provides a good match with the value obtained from ^{1}H DOSY NMR experiments. A lower value in electrochemical experiments is expected, given that the latter was performed in a more viscous medium of high ionic strength (0.5 M NBu_4^+ ClO_4^- in CH_2Cl_2) as opposed to neat CD_2Cl_2.

The origin of the third oxidation of **Ru$_6$-4** cannot be assigned unambiguously; it either constitutes the third oxidation of the three *m*-divinylphenylene-diruthenium clamps or the oxidation of the two TPA linkers. The lower current amplitude of this final redox process argues for TPA oxidation, but the broadening and proximity of this wave to the anodic discharge limit of the electrolyte do not allow for an accurate determination of associated peak currents.

For **Ru$_6$-5**, the third redox wave at $E_{1/2}$ = 680 mV is associated with the same peak currents as the first two waves. This is also demonstrated by the identical step heights in LSV as shown in Figure S18. The final, broader, and chemically only partially reversible oxidation at $E_{1/2}$ = 930 mV is associated with a smaller peak current. Accordingly, the step height as obtained from LSV amounts to two-thirds of that of the previous waves, suggesting an overall two-electron process and hence oxidation of the TPA linkers. All three or four redox processes are well-separated with half-wave potential splittings $\Delta E_{1/2}$ in the range of 250 to 605 mV, signaling that all redox states with equivalently charged linkers are thermodynamically stable species and do not engage to relevant extents in disproportionation reactions.

In order to identify the actual redox sites by monitoring the spectroscopic consequences of the stepwise oxidations and to verify the electron counts associated with each step, we performed IR–NIR and UV–vis–NIR spectroelectrochemical (SEC) measurements and redox titrations. The SEC experiments were conducted with a custom-made, optically transparent, thin-layer electrolysis (OTTLE) cell according to the design of Hartl et al.[80] These studies also probe the persistence of the various oxidized forms on a longer timescale than that encountered in CV experiments as the interconversion between different redox states within the diffusion layer of the SEC cell requires ca. 20–30 min for every step. Our IR studies capitalize on the intense and characteristic CO stretching vibrations of the ruthenium-bonded CO ligands, whose energies respond to the loss of electron density suffered by the {***Ru***} entities during the individual oxidation(s). Table 2 summarizes the data from these experiments, while those for the precursor complexes **Ru$_2$-2** and **Ru$_2$-3** are provided in Table S5.

Table 2. Spectroscopic Changes of Compounds Ru$_6$-4 and Ru$_6$-5 in the IR–NIR and UV–vis–NIR Spectra in Their Neutral, Tricationic, and Hexacationic States[a]

	ν_{CO} (cm^{-1})	λ (nm) (ε_{max}[in 10^3 $M^{-1}cm^{-1}$])
Ru$_6$-4	1900	332 (148), 345 (150)
[**Ru$_6$-4**]$^{3+}$	1907, 1962	362 (131), 417 (65), 668 (17), 1206 (6.2)
[**Ru$_6$-4**]$^{6+}$	1977	282 (84), 362 (95), 633 (14), 772 (11)
Ru$_6$-5	1900	316 (121), 353 (151)
[**Ru$_6$-5**]$^{3+}$	1918, 1938	356 (144), 463 (52), 667 (19), 1530 (14), 1955 (26)
[**Ru$_6$-5**]$^{6+}$	1946, 1967	361 (115), 413 (59), 461 (42), 803 (14), 1380 (36)

[a]Measurements were carried out in 1,2-$C_2H_4Cl_2$/NBu_4^+ PF_6^- at rt.

Neutral **Ru$_6$-4** has a single band at 1900 cm^{-1} for the stretching vibrations of the CO ligands. As a result of the higher 18 valence electron count at the ruthenium ions, this band is red-shifted by 10 cm^{-1} from that of its precursor **Ru$_2$-2** (Scheme 1).[66,77] One-electron oxidized [**Ru$_2$-2**]$^+$ showed two separate, similarly intense Ru(CO) bands, which were both shifted to higher energies with respect to neutral **Ru$_2$-2**. It was hence identified as an electronically moderately coupled mixed-valent (MV) system of Class II according to the classification scheme of Robin and Day.[81] The same situation also applies for **Ru$_6$-4**. After exhaustive electrolysis at a potential positive of the first composite redox wave, the single CO band was replaced by two equally intense, blue-shifted Ru(CO) bands at 1907 and 1962 cm^{-1} (see Figures S19–S21). A further asset of the oxidized form is a broad, weak (ε = 6200 M^{-1} cm^{-1}) intervalence charge-transfer (IVCT) band in the NIR (Figure S19), which is more clearly observed in the corresponding UV–vis–NIR experiment as a band peaking at 1206 nm (8290 cm^{-1}, see Figure S22).

On further increasing the potential at the working electrode past the half-wave potential of the second redox wave, the split Ru(CO) bands merged into a single, even further blue-shifted band at 1977 cm^{-1}, showing that, after this process, all {***Ru***} entities are again electronically equivalent. Concomitant with this process is the bleaching of the IVCT band. The CO band patterns and shifts and the NIR responses are fully congruent with those observed during the first and the second oxidations of **Ru$_2$-2**. This further supports our assignment of the first two waves to the coincident first and second oxidations of the *m*-divinylphenylene diruthenium clamps and hence stepwise formation of first [**Ru$_6$-4**]$^{3+}$ and then [**Ru$_6$-4**]$^{6+}$. From the stepwise CO band shifts, we can derive a charge distribution parameter $\Delta\rho$ as defined by Geiger et al.[82,83] of 0.14, which signals an unsymmetrical charge distribution of ca. 86%:14% over the two halves of every *m*-divinylphenylene diruthenium fragment in the MV trications. Further explanations as to how $\Delta\rho$ is determined and its physical meaning are provided in the Supporting Information. The present value of 0.14 for [**Ru$_6$-4**]$^{3+}$ is, within experimental accuracy, identical to 0.12 for [**Ru$_2$-2**]$^+$.[77]

Ru$_6$-5 showed a different response in the IR–NIR SEC experiments. The species formed after traversing the first composite wave was characterized by two less widely spaced Ru(CO) bands with a more intense feature at 1918 cm^{-1} and a less intense one at 1938 cm^{-1} (Figures 7 and S23). In addition, the IVCT band was much more intense (ε = 26 000 M^{-1} cm^{-1}) and exhibited vibrational structuring with separate peaks at 6537 cm^{-1} (1530 nm) and 5116 cm^{-1} (1955 nm). Both these features signal enhanced electronic coupling within the MV divinylphenylene diruthenium entities. Obviously, the electron-donating butoxy substituents increase the contributions of the *m*-divinylphenylene linker to the relevant redox orbitals further and aid in levelling the charge differences between the clamped {***Ru***} sites out. Just like for **Ru$_6$-4**, the latter IR and IVCT bands vanished completely after exhaustive electrolysis at a potential sufficiently positive of the second wave. The resulting spectrum exhibited a new Ru(CO) band at 1946 cm^{-1} with a higher energy shoulder at 1967 cm^{-1} (see Figure S24 for a deconvoluted IR spectrum), which here seem to represent the allowed out-of-phase and the normally symmetry-forbidden in-phase combinations of the Ru(CO) stretches.[84,85] Concomitant with the second oxidation, the structured NIR band, which corresponds to an electronic excitation within the π-conjugated open-shell divinylphenylene diruthenium chromophores, was bleached and replaced by a new, more intense band at 7245

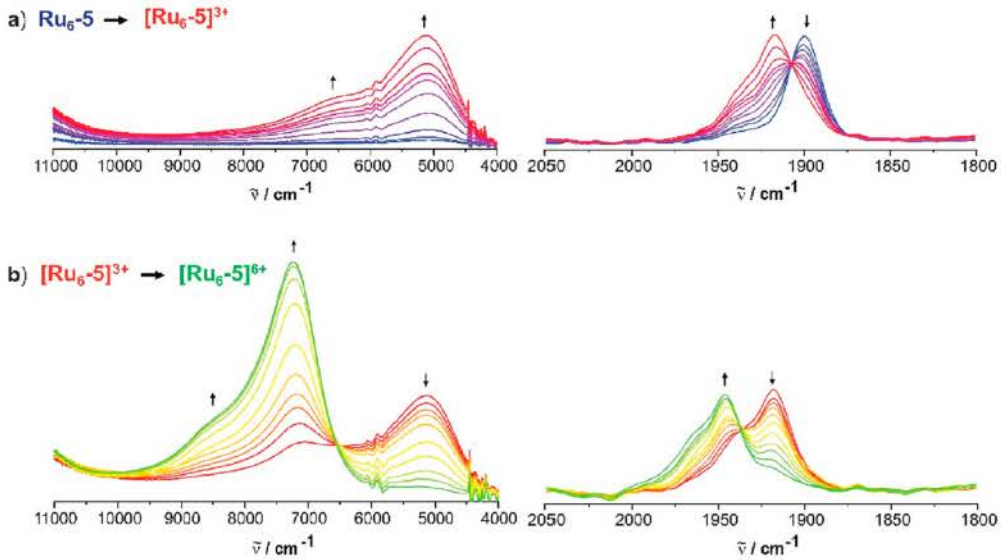

Figure 7. Changes of the absorption profiles in the NIR and in the region of the Ru(CO) stretching vibrations in the IR on stepwise in situ oxidation (a) past the first (top panel) and (b) positive of the second wave (bottom panel) of **Ru_6-5** in an OTTLE cell (0.1 M NBu_4^+ PF_6^- in 1,2-$C_2H_4Cl_2$ at rt).

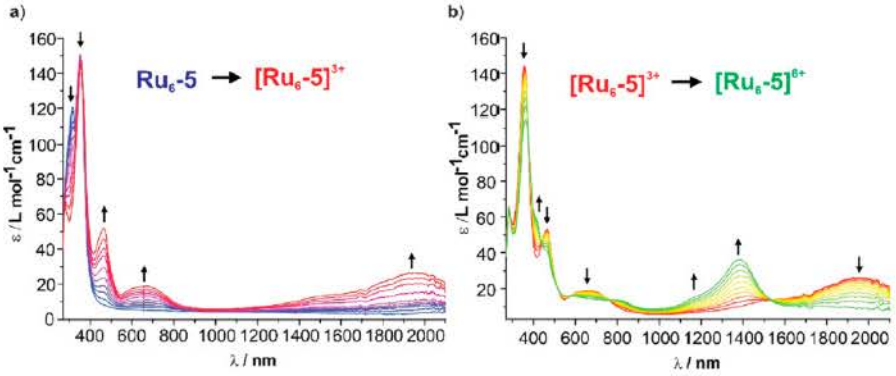

Figure 8. Spectroscopic changes in the UV–vis–NIR absorption spectra during electrolysis at a potential (a) positive of the first (left) and (b) positive of the second wave of **Ru_6-5** (right).

cm^{-1} (1380 nm) with a superimposed shoulder at 8475 cm^{-1} (1180 nm). The same behavior was encountered during stepwise oxidations of other divinylarylene diruthenium complexes and metallamacrocycles with electronically coupled MV states.[44,46–50,86–88]

Characteristic changes are also observed in the UV–vis regions of the electronic spectra. Neutral **Ru_6-5** exhibits two prominent electronic bands near 316 and 353 nm but is nearly transparent for visible light, thus showing only a pale-yellow color. Electrolysis past the potential of the first wave caused the UV band at the higher energy to vanish, while two new vis bands at 463 and 667 nm grew in along with the previously mentioned IVCT feature in the NIR (Figure 8). Further electrolysis at a potential positive of the second wave caused the vis band at 667 nm to decrease in intensity, while another more red-shifted band that peaks at 803 nm developed. Minor alterations were also observed in the UV and blue regions of the vis (Figure 8 and Table 2). Qualitatively similar stepwise changes were also found for its nonbutoxylated congener **Ru_6-4**. The spectra obtained after traversing the first and second composite waves are again similar to those recorded for the one- and two-electron oxidized forms of their dinuclear precursors **Ru_2-2** and **Ru_2-3** (see Table S5 of the Supporting Information). The main difference is that the extinction coefficients ε are roughly 3 times larger as a consequence of the presence of three such chromophores within the same molecule instead of just one.

As a final cross-check, we chemically oxidized **Ru_6-5** by adding, in increments of 0.5 equiv, an increasing number of aliquots of ferrocenium hexafluorophosphate to a standard amount of a solution of **Ru_6-5** that represented 1 equiv of the cage. The resulting solutions were then monitored by UV–vis–NIR spectroscopy. The redox potential $E_{1/2}$ of the ferrocenium oxidant of 0 mV is sufficiently positive of the first redox wave of this cage but is sufficiently negative of the second one to avoid overoxidation. The results of this study are shown in Figure 9. Full conversion of **Ru_6-5** to the species that was formed after exhaustive electrolysis at a potential positive of the first composite redox wave required 3 equiv of the one-electron ferrocenium oxidant; the addition of larger quantities had no further effect. The same species was also generated by adding 3 equiv of the stronger oxidant acetylferrocenium ($E_{1/2}$ = 0.27 V)[89] to **Ru_6-5**. The redox potential of this stronger oxidant is

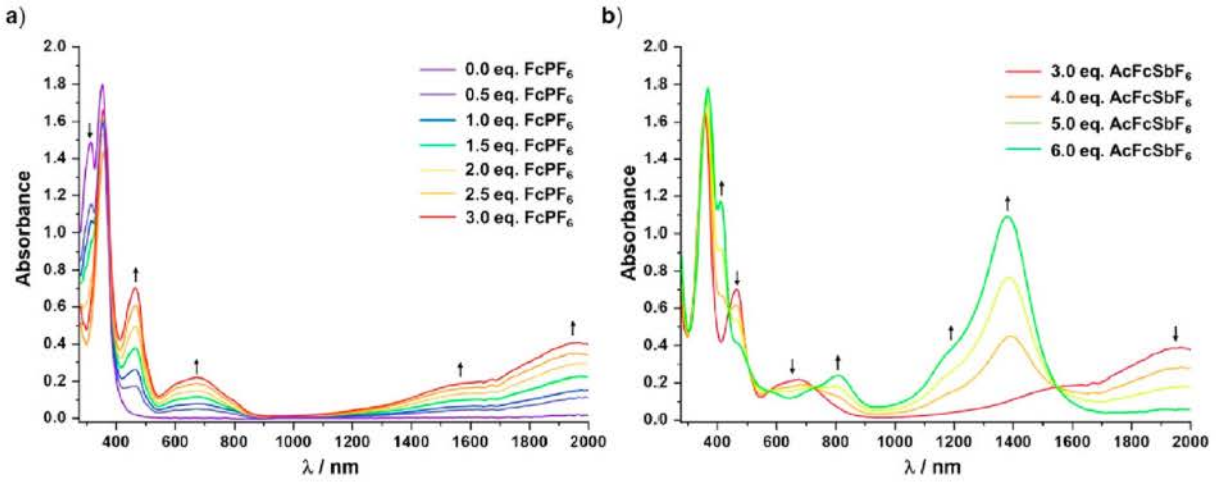

Figure 9. Redox titrations of cage **Ru_6-5** with (a) addition of increasing amounts (0.5 to 3 equivalents (equiv) of ferrocenium hexafluorophosphate and (b) 3 to 6 equiv of acetylferrocenium hexafluoroantimonate to 1 equiv of **Ru_6-5** in CH_2Cl_2.

sufficiently positive of the second redox potential of **Ru_6-5**. This allowed us to access also the higher oxidized form. Full conversion to the species that had resulted from exhaustive oxidation past the second redox wave of **Ru_6-5** required three additional equivalents of the acetylferrocenium salt. This finally establishes the three-electron nature of each of these two redox processes and, by inference from the CV and LSV data, also of the third oxidation of **Ru_6-5**. **Ru_6-4** and **Ru_6-5** are thus characterized by coincident oxidations of the three divinylphenylene diruthenium straps by first one and then a second or even a third electron. The lack of any IVCT absorption for electron transfer at intermediate stages where divinylphenylene-diruthenium entities are present in mutually different charge states indicates that the TPA tricarboxylate linkers behave as insulators. Such a situation is routinely encountered in metallamacrocycles with divinylarylene diruthenium entities and bridging aryldicarboxylate ligands[45−47,49,50] or in metallacages and metallamacrocycles with redox-active TTF-derived[67−72] or other redox-active constituents.[16,73−75]

We note that the changes encountered in the SEC experiments were reversible. Isosbestic points were retained over the entire processes (see Figures 7 and 8) and also in the redox titrations (Figure 9). Back electrolysis after exhaustive three- and sixfold oxidations provided the spectra of the neutral precursors in (nearly) quantitative spectroscopic yields. This shows that these cages are capable of releasing a total of six electrons and retain their cage structures with good stabilities over a period of 90 min or more. Similar cases of reversible multielectron transfer in cage compounds, in particular with redox-active tetrathiafulvalene-type linkers, were reported on previous occasions.[67,69,70,72] However, examples of a (reversible) redox-induced disassembly of discrete coordination cages into their individual constituents or their conversions into coordination polymers are also known.[90,91]

Attempts to also generate the higher oxidized forms of **Ru_6-5** inside an OTTLE cell led to a bleach of basically all vis−NIR bands and the replacement of the Ru(CO) band envelope of $[\mathbf{Ru_6\text{-}5}]^{6+}$ in favor of a single, new, and even further blue-shifted Ru(CO) band at 1983 cm^{-1}. However, these changes were irreversible so that this species did not revert to the pristine cage after applying a negative potential to the working electrode of the OTTLE cell. Similar results were obtained after chemically oxidizing **Ru_6-5** with 9 equiv of thianthrenium hexafluoroantimonate. The resulting electronic and IR spectra were identical to the ones obtained after electrochemical oxidation and gave an intense EPR signal at g = 1.999 with resolved hyperfine splittings to the ^{31}P atoms of two P^iPr_3 ligands and two $^{99/101}Ru$ nuclei (see Figure S34). These findings agree with the presence of an oxidized divinylarylene-bridged diruthenium complex with five-coordinated metal ions and with a symmetric charge and spin density distribution [note that an oxidation at the TPA linker would result in a single resonance line with no resolved hyperfine splittings (hfs) or a non-binomial triplet due to coupling with the ^{14}N nucleus]. The identity of this species remains, however obscure, as back reduction with 9 equiv of decamethylferrocene also did not provide the parent cage.

We also characterized the tri- and hexacations of cages **Ru_6-4** and **Ru_6-5** by means of EPR spectroscopy. As in the UV−vis−NIR titration experiments, stepwise addition of 0.5 equiv aliquots of the ferrocenium oxidant to a solution of **Ru_6-5** generated a broad, isotropic resonance signal at g = 2.011 without any resolved hfs to ^{31}P or ^{1}H nuclei, whose intensity scaled with the amount of added ferrocenium (see Figure S28). Such a signal is characteristic of an oxidized MV divinylarylene-bridged diruthenium complex with hexacoordinated metal entities and large "bridge" contributions to the singly occupied molecular orbital [SOMO(s)].[50,85,92] $[\mathbf{Ru_6\text{-}4}]^{3+}$, which was generated by oxidizing the parent neutral cage with 3 equiv of acetylferrocenium hexafluoroantimonate ($AcFc^+$ SbF_6^-), likewise shows an unstructured EPR resonance at slightly larger g value of 2.020 (Figure S29). In agreement with the results on dioxidized $[\mathbf{Ru_2\text{-}2}]^{2+}$, $[\mathbf{Ru_6\text{-}4}]^{6+}$ and $[\mathbf{Ru_6\text{-}5}]^{6+}$ exhibit a broader, less intense EPR signal at g = 2.038 or 2.020, respectively (see Figures S30 and S31). The slightly larger g values as compared to the trications signal a slightly larger metal contribution to the SOMO(s).[77] EPR spectra recorded on solutions of **Ru_6-5** that were treated with variable amounts of the $AcFc^+$ SbF_6^- oxidant are shown in Figure S32 and confirm that 6 equiv of the oxidant were needed for full conversion.

Chemical oxidation of the hexaruthenium cages can also be achieved with the strong organic acceptor F_4TCNQ, whose first reduction potential of 153 mV versus FcH/FcH^+ (under our

conditions) is well positive of the 0/3+ couples of both hexaruthenium cages. F_4TCNQ is a popular ingredient of so-called CT salts, in particular, in conjunction with planar polycyclic aromatic hydrocarbons as electron donors. Such CT salts have been widely investigated for the variable degrees of CT from the donor to the F_4TCNQ acceptor, the various stoichiometries D_mA_n (D = electron donor, A = electron acceptor) that can be realized, and the electronic and conductive properties of the ensuing compounds.[93−103] We have recently reported on CT salts that consist of the radical cation of a divinylarylene-bridged diruthenium complex and its macrocyclic analogue with a laterally π-extended divinylarylene or -phenanthrenylene linker and the F_4TCNQ^- radical anion.[85,104]

Treatment of cages **Ru_6-4** and **Ru_6-5** with 3 equiv of F_4TCNQ in CH_2Cl_2 accordingly yielded the radical salts $[\mathbf{Ru_6\text{-}4}]^{3+}$ $[\mathbf{F_4TCNQ^-}]_3$ (**CT-1**) and $[\mathbf{Ru_6\text{-}5}]^{3+}$ $[\mathbf{F_4TCNQ^-}]_3$ (**CT-2**) as sketched in Scheme 2. Their characterization by EPR, IR−NIR,

Scheme 2. Synthesis of the CT Salts CT-1 and CT-2 From Ru_6-4 and Ru_6-5 With F_4TCNQ

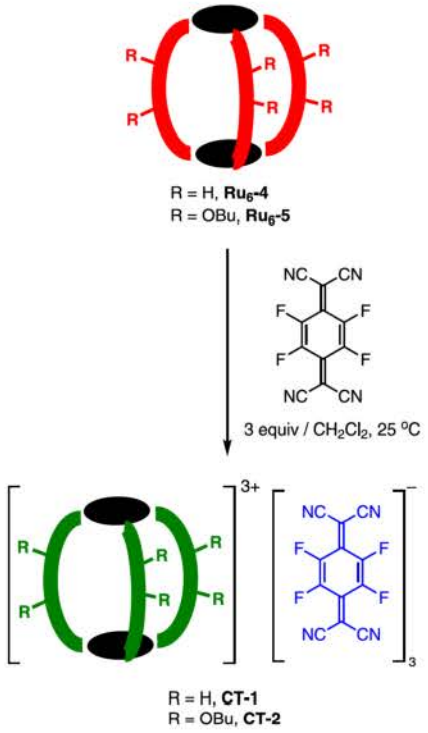

and UV−vis−NIR studies confirmed the presence of trioxidized cages and F_4TCNQ^- anions in these salts as depicted in Figure 10. For **CT-1**, the broad EPR signal of $[\mathbf{Ru_6\text{-}4}]^{3+}$ and the richly structured resonance of the F_4TCNQ^- anion at g = 1.9925 overlap, while in the case of **CT-2**, two signals were detected individually due to the decreased width of the resonance of the organometallic cage species. Both the CT salts showed the Ru(CO) bands of the trioxidized cages as well as the C≡N stretching vibrations of the F_4TCNQ^- anion at 2194 and 2175 cm^{-1}.[105,106] Likewise, the electronic spectra featured the characteristic, structured double peak of the latter anion at 866 and 770 nm along with the UV−vis and the NIR IVCT bands of the triply charged cages as obtained after exhaustive electrolysis past the half-wave potential of the first composite redox wave or by chemical oxidation of **Ru_6-5** with 3 equiv of FcH^+ PF_6^- (see Figures S34−S36). Unfortunately, we have not been able to obtain single crystals of these two salts that would allow for a further analysis of the cation/anion packing motifs and interion interactions.

CONCLUSIONS

In conclusion, we have demonstrated the synthesis of hexaruthenium cages **Ru_6-4** and **Ru_6-5** in high yields from *m*-divinylphenylene-bridged diruthenium complexes as ditopic metal clamps and triphenylamine-4,4′,4″-tricarboxylate as the tritopic linker. The cages are characterized by a twisted trigonal prismatic arrangement of the six ruthenium ions. They crystallize as racemates of the Δ- and Λ-enantiomers that differ by the sense of rotation (clockwise or counterclockwise) of the triangular faces of the distorted trigonal hexaruthenium prism with a rotational angle of ca. ±40°. The cages are redox-active and display three (**Ru_6-4**) or even four (**Ru_6-5**) well-separated redox waves which represent the coincident oxidations of the chemically equivalent divinylphenylene diruthenium clamps or the triphenylamine-4,4′,4″-tricarboxylate linkers. The cages thus have the propensity to release up to 11 electrons with (partially) reversible responses in CV. We could further demonstrate that the corresponding tri- and hexacations $[\mathbf{Ru_6\text{-}4}]^{3+}$, $[\mathbf{Ru_6\text{-}5}]^{3+}$ and $[\mathbf{Ru_6\text{-}4}]^{6+}$, $[\mathbf{Ru_6\text{-}5}]^{6+}$ can be (electro)chemically generated and characterized spectroscopically and persist for at least 90 min, whereas the higher oxidized forms degrade irreversibly. All oxidation states have distinct absorption profiles in the UV, visible (vis) and NIR regions of their electronic spectra, rendering the cages polyelectrochromic. The electron-donating butoxy groups stabilize the individual oxidized forms by 250 mV or more and provide a more balanced charge distribution within the singly oxidized, mixed-valent *m*-divinylphenylene diruthenium clamps, when compared to the unsubstituted phenylene congener. We also demonstrated that the cages form stable radical salts $[\mathbf{Ru_6\text{-}4/5}]^{3+}$ $[\mathbf{F_4TCNQ^-}]_3$ on treatment with 3 equiv of F_4TCNQ as a strong organic electron acceptor.

EXPERIMENTAL SECTION

General Methods. All manipulations were performed under an atmosphere of purified nitrogen with dry, distilled, and nitrogen-saturated solvents. All reagents were purchased from commercial sources and were used without further purification. 4,4′,4″-Triphenylamine-tribenzoic acid was obtained from Ambeed, Inc. ^{1}H NMR (400 MHz) and ^{31}P NMR (162 MHz) spectra were recorded on a Bruker AVANCE III 400 spectrometer; ^{1}H (600 MHz), ^{13}C (151 MHz), and ^{31}P (243 MHz) NMR spectra were recorded on a Bruker AVANCE III 600 spectrometer. ^{1}H NMR (800 MHz) and ^{13}C (202 MHz) NMR spectra were recorded on a Bruker AVANCE Neo 800 spectrometer. Precursor complexes **Ru_2-2**[77] and **Ru_2-3**[66] were prepared according to the previously reported procedures.

Mass spectra were recorded on an UHR-ToF Bruker Daltonik (Bremen, Germany) maXis ESI-quadrupole time-of-flight (qToF) mass spectrometer with a resolution better than 60.000 full width at half-maximum. The N_2 drying gas was heated to 180 °C, while the spray gas temperature was 20 °C. Signal detection was done in the positive ion mode at a 4.5 kV voltage. Calibration with the ESI-ToF low concentration tuning mix of Agilent was performed prior to every measurement. All measurements were performed on CH_2Cl_2 solutions of the respective complex.

Electrochemical and SEC Measurements. Electrochemical experiments were performed in a custom-made cylindrical vacuum-tight one-compartment cell. A spiral-shaped Pt wire and an Ag wire as the counter and reference electrodes were sealed into glass capillaries

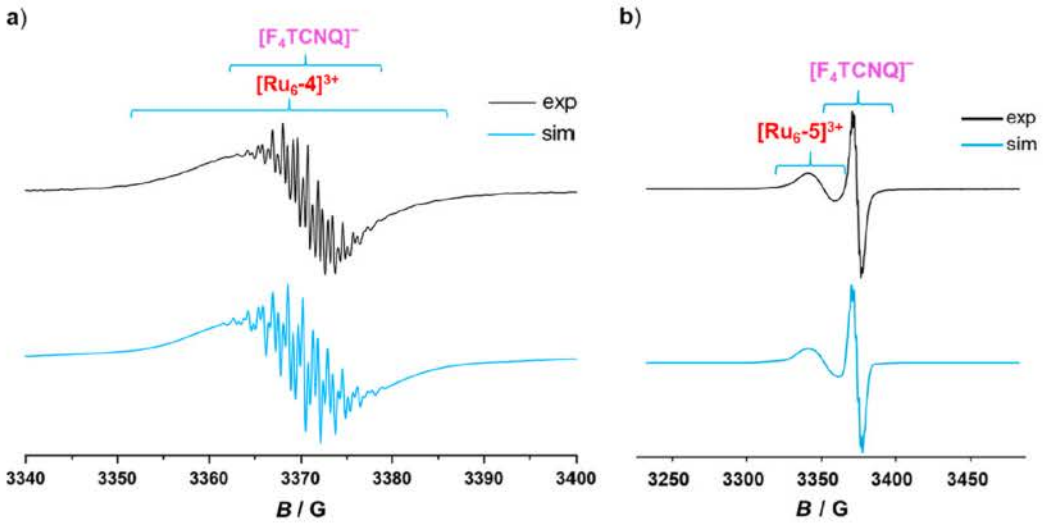

Figure 10. EPR spectra of salts (a) **CT-1** and (b) **CT-2** synthesized from $\mathbf{Ru_6}$**-4** and $\mathbf{Ru_6}$**-5** and 3 equiv of F_4TCNQ. The experimental spectra (black lines) are shown at the top and the simulated ones (blue lines) at the bottom.

that were introduced via Quickfit screws at opposite sides of the cell. A platinum electrode was introduced as the working electrode through the top port via a Teflon screw cap with a suitable fitting. It was polished first with 1 μm and then with 0.25 μm diamond paste from Buehler-Wirtz before the measurements. The cell was attached to a conventional Schlenk line via a side arm, which was equipped with a Teflon screw valve. The cell allowed the experiments to be performed under an atmosphere of argon with approximately 7 mL of analyte solution. NBu_4^+ PF_6^- (0.1 M) was used as a supporting electrolyte. Referencing was done by the addition of decamethylferrocene (DMFc) as an internal standard to the analyte solution after all data of interest had been acquired. Representative sets of scans were repeated with the added standard. Final referencing was done against the ferrocene/ferrocenium ($FcH^{0/+}$) couple with $E_{1/2}(DMFc^{0/+}) = -550$ mV versus $E_{1/2}(FcH^{0/+})$ when NBu_4^+ PF_6^- was used as the supporting electrolyte. Chronoamperometry was performed on a MF-2012 glassy carbon disc electrode with a diameter of 3 mm from BASi with a step time of 2 s. LSV employed a MF-2005 platinum microelectrode with a diameter of 10 μm from the same manufacturer. Sweeps were performed at scan rates of 10, 5, and 3 mV s^{-1} to ensure radial diffusion and the scan-rate independence of the limiting currents. Then, the diffusion coefficient of $\mathbf{Ru_6}$**-5** was measured under the same conditions as those utilized by Swaddle and co-workers (0.5 M NBu_4^+ ClO_4^- in CH_2Cl_2, r. t.) for measuring the diffusion coefficient of DMFc.[79] The literature value D_{DMFc} of 10.7×10^{-10} m^2 s^{-1} was used for determining the surface area A of the working electrode. Electrochemical data were acquired with a computer-controlled BASi potentiostat. The OTTLE cell was also custom-made and comprises of a Pt-mesh working and counter electrode and a thin silver wire as a pseudoreference electrode sandwiched between the CaF_2 windows of a conventional liquid IR cell. Its design follows that of Hartl et al.[80] The working electrode is positioned in the center of the spectrometer beam.

FT-IR spectra were recorded on a Bruker TensorIII instrument. UV−vis−NIR spectra were obtained on a TIDAS fiberoptic diode array spectrometer (combined MCS UV-NIR and PGS NIR instrumentation) from J&M in HELLMA quartz cuvettes with 0.1 cm optical path lengths. EPR studies were performed on a table-top X-band spectrometer MiniScope MS 400 from Magnettec. Simulation of the experimental EPR spectra was performed with the MATLAB EasySpin program.[107] All measurements were performed at rt, and the diruthenium complexes were chemically oxidized using ferrocenium hexafluorophosphate (FcH^+ PF_6^-), acetylferrocenium hexafluoroantimonate ($AcFc^+$ SbF_6^-), or thianthrenium hexafluoroantimonate as oxidizing agents. Thianthrenium hexafluoroantimonate was synthesized according to a reported procedure.[108]

X-ray Crystallography. X-ray diffraction analysis was performed on a STOE IPDS-II diffractometer (STOE & CIE GmbH, Darmstadt, Germany) equipped with a graphite-monochromated MoK_α radiation source (λ = 0.71073 Å) and an image plate detection system at T = 100.15 K. Using Olex2,[109] the structures were solved with the ShelXT[110] structure solution program using Intrinsic Phasing and refined with the ShelXL[110] refinement package using least-squares minimization. Hydrogen atoms were introduced at their calculated positions. Structure plots were generated with the Mercury[111] and PyMOL[112] programs.

Compound Synthesis and Characterization. *Synthesis of* $\mathbf{Ru_6}$*-4.*

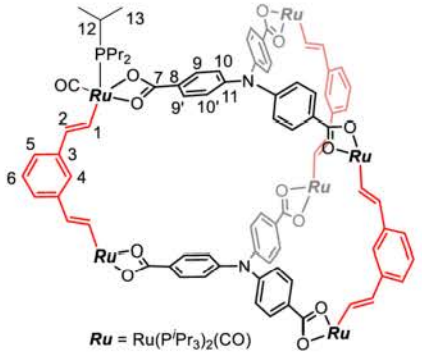

In a 25 mL flask, 4,4′,4″-triphenylamine-tricarboxylic acid (12.5 mg, 0.033 mmol) and potassium carbonate (16 mg, 0.116 mmol) were dissolved in methanol (7 mL). The solution was stirred for 3 h at ambient temperature. The solution of deprotonated 4,4′,4″-triphenylamine-tricarboxylate was added dropwise into a dichloromethane solution of diruthenium complex $\mathbf{Ru_2}$**-2** (52 mg, 0.047 mmol) over the course of 15 min. Subsequently, the reaction mixture was warmed to 40 °C and stirred for 30 h. After evaporating the solvent under reduced pressure, the light green solid of $\mathbf{Ru_6}$**-4** was collected and washed with methanol to remove KCl (3 × 2 mL) and with hexane (3 × 2 mL). Yield: 57.3 mg (0.015 mmol, 93%).

^{1}H NMR (800 MHz, CD_2Cl_2): δ = 8.99 (d, $^3J_{H,H}$ = 15.3 Hz, 6H, H_1), 8.06 (d, $^3J_{H,H}$ = 8.0 Hz, 6H, $H_{9/9'}$), 7.95 (d, $^3J_{H,H}$ = 8.0 Hz, 6H, $H_{9/9'}$), 7.65 (s, 3H, H_4), 7.29 (d, $^3J_{H,H}$ = 8.0 Hz, 6H, $H_{10/10'}$), 7.11−7.05 (m, 9H, H_6, $H_{10/10'}$), 6.61 (dd, $^3J_{H,H}$ = 7.6 Hz, $^4J_{H,H}$ = 1.1 Hz, 6H, H_5), 6.25 (d, $^3J_{H,H}$ = 15.3 Hz, 6H, H_2), 2.53−2.43 (m, 36H, H_{12}), 1.50−1.33 (m, 216H, H_{13}) ppm. $^{13}C\{^1H\}$ NMR (200 MHz, CD_2Cl_2): δ in ppm = 208.9 (t, $^2J_{C,P}$ = 15.2 Hz, Ru−CO), 175.6 (C_7), 160.1 (t, $^2J_{C,P}$ = 14.0 Hz, C_1), 149.8 (C8), 140.8 (C3), 133.7 (C2), 130.2, 129.8 (C10/10′), 129.2 (C11), 127.9 (C6), 124.0, 122.9 (C9/9′), 120.3 (C5), 117.6 (C4), 24.9−24.7 (C12), 19.7−19.5 (C13) ppm. $^{31}P\{^1H\}$ NMR (324 MHz, CD_2Cl_2): δ in ppm = 38.20, 37.81 (each d, $^2J_{PP}$ = 275 Hz, $\underline{P}^iPr_3$) ppm. IR (CH_2Cl_2): 1900 ($\nu_{C\equiv O}$) cm^{-1}. ESI-MS (+ve ion mode, CH_2Cl_2), *m/z*: 1915.6789 (calcd. $[M]^{2+}$ for $C_{186}H_{300}N_2O_{18}P_{12}Ru_6$ = 1915.6917), 3830.3612 (calcd. $[M - H]^+$ for $C_{186}H_{299}N_2O_{18}P_{12}Ru_6$ = 3830.3754), 3870.3252 (calcd. $[M + 2H + Cl]^+$ for $C_{186}H_{302}ClN_2O_{18}P_{12}Ru_6$ = 3870.3573).

Synthesis of ***Ru$_6$-5***.

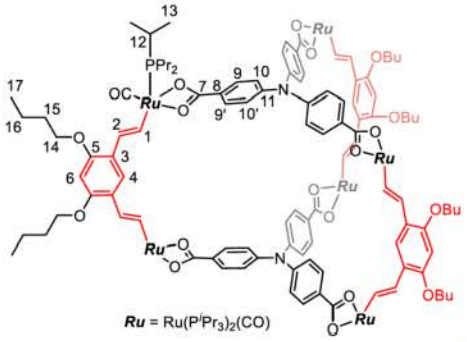

To a 50 mL flask, 4,4′,4″-triphenylamine-tricarboxylic acid (12.5 mg, 0.034 mmol) and potassium carbonate (16 mg, 0.116 mmol) were dissolved in methanol (7 mL). The solution was stirred for 3 h at ambient temperature. The solution of deprotonated 4,4′,4″-triphenylamine-tricarboxylate was added dropwise into a dichloromethane solution of diruthenium complex **Ru$_2$-3** (59 mg, 0.048 mmol) over the course of 15 min. Subsequently, the reaction mixture was warmed to 40 °C and stirred for 30 h. After evaporating the solution under reduced pressure, the light green solid of **Ru$_6$-5** was collected and washed with methanol (3 × 2 mL) and hexane (3 × 2 mL). Yield: 62.3 mg (0.015 mmol, 90%).

^{1}H NMR (800 MHz, CD_2Cl_2): δ = 8.60 (d, $^3J_{H,H}$ = 15.2 Hz, 6H, H_1), 8.05 (d, $^3J_{H,H}$ = 8.3 Hz, 6H, $H_{9/9'}$), 7.95 (d, $^3J_{H,H}$ = 8.3 Hz, 6H, $H_{9/9'}$), 7.55 (s, 3H, H_4), 7.28 (d, $^3J_{H,H}$ = 8.3 Hz, 6H, $H_{10/10'}$), 7.09 (d, $^3J_{H,H}$ = 8.3 Hz, 6H, $H_{10/10'}$), 6.54 (d, $^3J_{H,H}$ = 15.2 Hz, 6H, H_2), 6.42 (s, 3H, H_6), 4.05−3.95 (m, 12H, H_{14}), 2.58−2.44 (m, 36H, H_{12}), 1.92−1.84 (m, 12H, H_{15}), 1.68−1.62 (m, 12H, H_{16}), 1.52−1.30 (m, 216H, H_{13}), 1.13−1.05 (m, 18H, H_{17}) ppm. $^{13}C\{^1H\}$ NMR (200 MHz, CD_2Cl_2): δ = 209.0 (t, $^2J_{C,P}$ = 15.2 Hz, Ru−CO), 175.3 (C_7), 155.5 (t, $^2J_{C,P}$ = 14 Hz, C_1), 150.3 (C5), 149.6 (C8), 130.18, 129.77 (C10/10′), 129.2 (C11), 126.5 (C2), 123.88 (C9/9′), 123.70 (C4), 122.9 (C9/9′), 120.3 (C3), 99.3 (C6), 68.8 (C14), 31.9 (C15), 24.9−24.6 (C12), 19.9−19.4 (C13, C16), 14.1 (C17) ppm. $^{31}P\{^1H\}$ NMR (324 MHz, CD_2Cl_2): δ = 37.88, 37.25 (each d, $^2J_{PP}$ = 277 Hz, $\underline{P}^iPr_3$) ppm. IR (CH_2Cl_2): 1900 ($\nu_{C\equiv O}$) cm^{-1}. ESI-MS (+ve ion mode, CH_2Cl_2), *m/z*: 2131.8525 (calcd. $[M]^{2+}$ for $C_{210}H_{348}N_2O_{24}P_{12}Ru_6$ = 2131.8647); 1421.2332 (calcd. $[M]^{3+}$ for $C_{210}H_{348}N_2O_{24}P_{12}Ru_6$ = 1421.2430).

For stepwise oxidation to $[$**Ru$_6$-5**$]^{3+}$, a solution of **Ru$_6$-5** (4.27 mg, 0.001 mmol) in dichloromethane (6 mL) was prepared. In another flask, a solution of the oxidant ferrocenium hexafluorophosphate (FcH^+ PF_6^-, 1.66 mg, 0.005 mmol) was also prepared in dichloromethane (5 mL). According to Table 3, one aliquot of **Ru$_6$-5** was mixed with corresponding aliquots of the oxidant solution in a right proportion to get the desired ratio. CH_2Cl_2 was added until a total volume of 1.5 mL was obtained.

Table 3. Details to the Redox Titration for the Stepwise Oxidation of Ru$_6$-5 to $[$Ru$_6$-5$]^{3+}$

sl no.	vol. of **Ru$_6$-5** sol. (mL)	amount of **Ru$_6$-5** (mmol)	vol. of FcH^+ PF_6^- sol. (mL)	amount of FcH^+ PF_6^- (mmol)	vol. of CH_2Cl_2 added (mL)	total vol. (mL)	equiv.
1	1	0.00017	0.083	0.000085	0.42	1.5	1:0.5
2	1	0.00017	0.16	0.00017	0.34	1.5	1:1
3	1	0.00017	0.25	0.00025	0.25	1.5	1:1.5
4	1	0.00017	0.34	0.00034	0.16	1.5	1:2
5	1	0.00017	0.42	0.00043	0.083	1.5	1:2.5
6	1	0.00017	0.5	0.00051		1.5	1:3

The stepwise oxidations from $[$**Ru$_6$-5**$]^{3+}$ to $[$**Ru$_6$-5**$]^{6+}$ were performed as follows: A solution of $[$**Ru$_6$-5**$]^{3+}$ was prepared first by taking **Ru$_6$-5** (2.85 mg, 0.00068 mmol) and 3 equiv of the oxidant acetylferrocenium hexafluoroantimonate (0.94 mg, 0.00204 mmol) in dichloromethane (4 mL). In a separate flask, a solution of acetylferrocenium hexafluoroantimonate (2.3 mg, 0.005 mmol) in dichloromethane (5 mL) was prepared. Subsequently, the solution of $[$**Ru$_6$-5**$]^{3+}$ was mixed with appropriate amounts of the oxidant solution to get the desired ratio (see Table 4). Finally, CH_2Cl_2 was added to arrive at a total volume of 1.5 mL.

Table 4. Details to the Redox Titration for the Stepwise Oxidation of $[$Ru$_6$-5$]^{3+}$ to $[$Ru$_6$-5$]^{6+}$

sl no.	vol. of $[$**Ru6-5**$]^{3+}$ sol. (mL)	amount of $[$**Ru6-5**$]^{3+}$ (mmol)	vol. of $AcFc^+$ SbF_6^- sol. (mL)	amount of $AcFc^+$ SbF_6^- (mmol)	vol. of CH_2Cl_2 added (mL)	total vol. (mL)	equiv.
1	1	0.00017			0.5	1.5	1:3
2	1	0.00017	0.16	0.00017	0.34	1.5	1:4
3	1	0.00017	0.33	0.00034	0.16	1.5	1:5
4	1	0.00017	0.5	0.00051		1.5	1:6

Synthesis of CT Salts. Dichloromethane solutions of complexes **Ru$_6$-4**, **Ru$_6$-5**, and F_4TCNQ were prepared in separate flasks. Then, for the synthesis of CT salts, 1 equiv of the complex and 3 equiv of F_4TCNQ were mixed. An immediate color change from light green to green (for $[$**Ru$_6$-4**$]^{3+}$ $[$**F$_4$TCNQ$^-$**$]_3$) or from light yellow to dark green (for $[$**Ru$_6$-5**$]^{3+}$ $[$**F$_4$TCNQ$^-$**$]_3$) was observed. $[$**Ru$_6$-5**$]^{3+}$ $[$**F$_4$TCNQ$^-$**$]_3$ was characterized by EPR, IR, and UV−vis−NIR spectroscopies. Due to the poor solubility of $[$**Ru$_6$-4**$]^{3+}$ $[$**F$_4$TCNQ$^-$**$]_3$, satisfactory UV−vis−NIR data could not be obtained in solution.

■ ASSOCIATED CONTENT

Supporting Information

The Supporting Information is available free of charge at https://pubs.acs.org/doi/10.1021/acs.inorgchem.2c01608.

NMR spectra (including ^{1}H−^{1}H−COSY and ^{1}H DOSY), mass spectra, cyclic voltammograms, linear sweep voltammogram of **Ru$_6$-5**, details of the X-ray structure determinations, redox titrations, additional displays of SEC experiments, EPR spectra, ^{1}H, ^{13}C, and ^{31}P NMR spectra, HR ESI mass spectra, X-ray crystallographic information for **Ru$_6$-4** (CCDC 2163402) and **Ru$_6$-5** (2163413), plots of the spectroscopic changes monitored by IR/NIR- and UV−vis−NIR spectroelectrochemistry, deconvoluted spectra for the Ru(CO) bands, EPR spectra of the various oxidized forms, and the IR and EPR spectra of the F_4TCNQ^- salts of metallacages **Ru$_6$-4** and **Ru$_6$-5** (PDF)

Accession Codes

CCDC 2163402 and 2163413 contain the supplementary crystallographic data for this paper. These data can be obtained free of charge via www.ccdc.cam.ac.uk/data_request/cif, or by emailing data_request@ccdc.cam.ac.uk, or by contacting The Cambridge Crystallographic Data Centre, 12 Union Road, Cambridge CB2 1EZ, UK; fax: +44 1223 336033.

AUTHOR INFORMATION

Corresponding Authors

Rajorshi Das − *Fachbereich Chemie, Universität Konstanz, 78457 Konstanz, Germany*; Email: rajorshi.das@uni-konstanz.de

Rainer F. Winter − *Fachbereich Chemie, Universität Konstanz, 78457 Konstanz, Germany*; orcid.org/0000-0001-8381-0647; Email: rainer.winter@uni-konstanz.de

Authors

Michael Linseis − *Fachbereich Chemie, Universität Konstanz, 78457 Konstanz, Germany*

Stefan Scheerer − *Fachbereich Chemie, Universität Konstanz, 78457 Konstanz, Germany*

Katrin Zoller − *Fachbereich Chemie, Universität Konstanz, 78457 Konstanz, Germany*

Laura Senft − *Department Chemie, Ludwig-Maximilians Universität München, 81377 München, Germany*

Ivana Ivanović-Burmazović − *Department Chemie, Ludwig-Maximilians Universität München, 81377 München, Germany*

Notes

The authors declare no competing financial interest.

ACKNOWLEDGMENTS

We are indebted to the German Research Foundation (Deutsche Forschungsgemeinschaft, DFG) for the financial support of this work through grant Wi1262/17-1.

REFERENCES

(1) Gao, W. X.; Feng, H. J.; Guo, B. B.; Lu, Y.; Jin, G. X. Coordination-Directed Construction of Molecular Links. *Chem. Rev.* **2020**, *120*, 6288−6325.

(2) Cook, T. R.; Stang, P. J. Recent Developments in the Preparation and Chemistry of Metallacycles and Metallacages via Coordination. *Chem. Rev.* **2015**, *115*, 7001−7045.

(3) Smulders, M. M.; Riddell, I. A.; Browne, C.; Nitschke, J. R. Building on architectural principles for three-dimensional metallosupramolecular construction. *Chem. Soc. Rev.* **2013**, *42*, 1728−1754.

(4) Chakrabarty, R.; Mukherjee, P. S.; Stang, P. J. Supramolecular coordination: self-assembly of finite two- and three-dimensional ensembles. *Chem. Rev.* **2011**, *111*, 6810−6918.

(5) Fujita, M.; Tominaga, M.; Hori, A.; Therrien, B. Coordination Assemblies from a Pd(II)-Cornered Square Complex. *Acc. Chem. Res.* **2005**, *38*, 369−378.

(6) Han, M.; Engelhard, D. M.; Clever, G. H. Self-assembled coordination cages based on banana-shaped ligands. *Chem. Soc. Rev.* **2014**, *43*, 1848−1860.

(7) Han, Y. F.; Jia, W. G.; Yu, W. B.; Jin, G. X. Stepwise formation of organometallic macrocycles, prisms and boxes from Ir, Rh and Ru-based half-sandwich units. *Chem. Soc. Rev.* **2009**, *38*, 3419−3434.

(8) Ji, Z.; Wang, H.; Canossa, S.; Wuttke, S.; Yaghi, O. M. Pore Chemistry of Metal−Organic Frameworks. *Adv. Funct. Mater.* **2020**, *30*, 2000238.

(9) Alhasan, S.; Carriveau, R.; Ting, D. S. K. A review of adsorbed natural gas storage technologies. *Int. J. Environ. Stud.* **2016**, *73*, 343−356.

(10) Furukawa, H.; Cordova, K. E.; O'Keeffe, M.; Yaghi, O. M. The chemistry and applications of metal-organic frameworks. *Science* **2013**, *341*, 1230444.

(11) Rosi, N. L.; Eckert, J.; Eddaoudi, M.; Vodak, D. T.; Kim, J.; O'Keeffe, M.; Yaghi, O. M. Hydrogen Storage in Microporous Metal-Organic Frameworks. *Science* **2003**, *300*, 1127−1129.

(12) Yaghi, O. M.; O'Keeffe, M.; Ockwig, N. W.; Chae, H. K.; Eddaoudi, M.; Kim, J. Reticular synthesis and the design of new materials. *Nature* **2003**, *423*, 705−714.

(13) Shanmugaraju, S.; Joshi, S. A.; Mukherjee, P. S. Self-Assembly of Metallamacrocycles Using a Dinuclear Organometallic Acceptor: Synthesis, Characterization, and Sensing Study. *Inorg. Chem.* **2011**, *50*, 11736−11745.

(14) Xu, L.; Wang, Y.-X.; Yang, H.-B. Recent advances in the construction of fluorescent metallocycles and metallocages via coordination-driven self-assembly. *Dalton Trans.* **2015**, *44*, 867−890.

(15) Saha, M. L.; Yan, X.; Stang, P. J. Photophysical Properties of Organoplatinum(II) Compounds and Derived Self-Assembled Metallacycles and Metallacages: Fluorescence and its Applications. *Acc. Chem. Res.* **2016**, *49*, 2527−2539.

(16) Laramée-Milette, B.; Nastasi, F.; Puntoriero, F.; Campagna, S.; Hanan, G. S. Photo-Induced Assembly of a Luminescent Tetraruthenium Square. *Chem.—Eur. J.* **2017**, *23*, 16497−16504.

(17) Acharyya, K.; Bhattacharyya, S.; Sepehrpour, H.; Chakraborty, S.; Lu, S.; Shi, B.; Li, X.; Mukherjee, P. S.; Stang, P. J. Self-Assembled Fluorescent Pt(II) Metallacycles as Artificial Light-Harvesting Systems. *J. Am. Chem. Soc.* **2019**, *141*, 14565−14569.

(18) Zhang, Z.; Zhao, Z.; Wu, L.; Lu, S.; Ling, S.; Li, G.; Xu, L.; Ma, L.; Hou, Y.; Wang, X.; Li, X.; He, G.; Wang, K.; Zou, B.; Zhang, M. Emissive Platinum(II) Cages with Reverse Fluorescence Resonance Energy Transfer for Multiple Sensing. *J. Am. Chem. Soc.* **2020**, *142*, 2592−2600.

(19) Pilgrim, B. S.; Champness, N. R. Metal-Organic Frameworks and Metal-Organic Cages—A Perspective. *ChemPlusChem* **2020**, *85*, 1842−1856.

(20) Dong, J.; Shen, P.; Ying, S.; Li, Z.-J.; Yuan, Y. D.; Wang, Y.; Zheng, X.; Peh, S. B.; Yuan, H.; Liu, G.; Cheng, Y.; Pan, Y.; Shi, L.; Zhang, J.; Yuan, D.; Liu, B.; Zhao, Z.; Tang, B. Z.; Zhao, D. Aggregation-Induced Emission-Responsive Metal−Organic Frameworks. *Chem. Mater.* **2020**, *32*, 6706−6720.

(21) Jiao, J.; Li, Z.; Qiao, Z.; Li, X.; Liu, Y.; Dong, J.; Jiang, J.; Cui, Y. Design and self-assembly of hexahedral coordination cages for cascade reactions. *Nat. Commun.* **2018**, *9*, 4423.

(22) Feng, H. T.; Yuan, Y. X.; Xiong, J. B.; Zheng, Y. S.; Tang, B. Z. Macrocycles and cages based on tetraphenylethylene with aggregation-induced emission effect. *Chem. Soc. Rev.* **2018**, *47*, 7452−7476.

(23) Yan, X.; Cook, T. R.; Wang, P.; Huang, F.; Stang, P. J. Highly emissive platinum(II) metallacages. *Nat. Chem.* **2015**, *7*, 342−348.

(24) Shustova, N. B.; McCarthy, B. D.; Dincă, M. Turn-on fluorescence in tetraphenylethylene-based metal-organic frameworks: an alternative to aggregation-induced emission. *J. Am. Chem. Soc.* **2011**, *133*, 20126−20129.

(25) Pullen, S.; Tessarolo, J.; Clever, G. H. Increasing structural and functional complexity in self-assembled coordination cages. *Chem. Sci.* **2021**, *12*, 7269−7293.

(26) Nguyen, B. T.; Thoburn, J. D.; Grommet, A. B.; Howe, D. J.; Ronson, T. K.; Ryan, H. P.; Bolliger, J. L.; Nitschke, J. R. Coordination Cages Selectively Transport Molecular Cargoes Across Liquid Membranes. *J. Am. Chem. Soc.* **2021**, *143*, 12175−12180.

(27) Liu, Y.; Qiu, X.; Soni, S.; Chiechi, R. C. Charge transport through molecular ensembles: Recent progress in molecular electronics. *Chem. Phys. Rev.* **2021**, *2*, 021303.

(28) Grozema, F. C.; Houarner-Rassin, C.; Prins, P.; Siebbeles, L. D. A.; Anderson, H. L. Supramolecular Control of Charge Transport in Molecular Wires. *J. Am. Chem. Soc.* **2007**, *129*, 13370−13371.

(29) Xue, Y.; Hang, X.; Ding, J.; Li, B.; Zhu, R.; Pang, H.; Xu, Q. Catalysis within coordination cages. *Coord. Chem. Rev.* **2021**, *430*, 213656.
(30) Chu, D.; Gong, W.; Jiang, H.; Tang, X.; Cui, Y.; Liu, Y. Boosting Enantioselectivity of Chiral Molecular Catalysts with Supramolecular Metal-Organic Cages. *CCS Chem.* **2022**, *4*, 1180−1189.
(31) Mozaceanu, C.; Taylor, C. G. P.; Piper, J. R.; Argent, S. P.; Ward, M. D. Catalysis of an Aldol Condensation Using a Coordination Cage. *Chemistry* **2020**, *2*, 22−32.
(32) Morimoto, M.; Bierschenk, S. M.; Xia, K. T.; Bergman, R. G.; Raymond, K. N.; Toste, F. D. Advances in supramolecular host-mediated reactivity. *Nat. Catal.* **2020**, *3*, 969−984.
(33) Tan, C.; Chu, D.; Tang, X.; Liu, Y.; Xuan, W.; Cui, Y. Supramolecular Coordination Cages for Asymmetric Catalysis. *Chem.—Eur. J.* **2019**, *25*, 662−672.
(34) Fang, Y.; Powell, J. A.; Li, E.; Wang, Q.; Perry, Z.; Kirchon, A.; Yang, X.; Xiao, Z.; Zhu, C.; Zhang, L.; Huang, F.; Zhou, H. C. Catalytic reactions within the cavity of coordination cages. *Chem. Soc. Rev.* **2019**, *48*, 4707−4730.
(35) Mouarrawis, V.; Plessius, R.; van der Vlugt, J. I.; Reek, J. N. H. Confinement Effects in Catalysis Using Well-Defined Materials and Cages. *Front. Chem.* **2018**, *6*, 623.
(36) Cullen, W.; Metherell, A. J.; Wragg, A. B.; Taylor, C. G. P.; Williams, N. H.; Ward, M. D. Catalysis in a Cationic Coordination Cage Using a Cavity-Bound Guest and Surface-Bound Anions: Inhibition, Activation, and Autocatalysis. *J. Am. Chem. Soc.* **2018**, *140*, 2821−2828.
(37) Schulze, M.; Kunz, V.; Frischmann, P. D.; Würthner, F. A supramolecular ruthenium macrocycle with high catalytic activity for water oxidation that mechanistically mimics photosystem II. *Nat. Chem.* **2016**, *8*, 576.
(38) Kunz, V.; Lindner, J. O.; Schulze, M.; Röhr, M. I. S.; Schmidt, D.; Mitrić, R.; Würthner, F. Cooperative water oxidation catalysis in a series of trinuclear metallosupramolecular ruthenium macrocycles. *Energy Environ. Sci.* **2017**, *10*, 2137−2153.
(39) Meza-Chincha, A.-L.; Schindler, D.; Natali, M.; Würthner, F. Effects of Photosensitizers and Reaction Media on Light-Driven Water Oxidation with Trinuclear Ruthenium Macrocycles. *ChemPhotoChem* **2021**, *5*, 173−183.
(40) Gao, W.-X.; Zhang, H.-N.; Jin, G.-X. Supramolecular catalysis based on discrete heterometallic coordination-driven metallacycles and metallacages. *Coord. Chem. Rev.* **2019**, *386*, 69−84.
(41) Sadjadi, S. Supramolecular Coordination Cages as Nanoreactors. In *Organic Nanoreactors*; Sadjadi, S., Ed; Academic Press: Boston, 2016; pp 257−303. DOI: 10.1016/b978-0-12-801713-5.00009-4
(42) Noh, T. H.; Jung, O.-S. Recent Advances in Various Metal−Organic Channels for Photochemistry beyond Confined Spaces. *Acc. Chem. Res.* **2016**, *49*, 1835−1843.
(43) Gao, X.; Cui, Z.; Shen, Y.-R.; Liu, D.; Lin, Y.-J.; Jin, G.-X. Synthesis and Near-Infrared Photothermal Conversion of Discrete Supramolecular Topologies Featuring Half-Sandwich [Cp*Rh] Units. *J. Am. Chem. Soc.* **2021**, *143*, 17833−17842.
(44) Fink, D.; Staiger, A.; Orth, N.; Linseis, M.; Ivanović-Burmazović, I.; Winter, R. F. Redox-Induced Hydrogen Bond Reorientation Mimicking Electronic Coupling in Mixed-Valent Diruthenium and Macrocyclic Tetraruthenium Complexes. *Inorg. Chem.* **2020**, *59*, 16703−16715.
(45) Fink, D.; Orth, N.; Linseis, M.; Ivanović-Burmazović, I.; Winter, R. F. Structural Versatility and Supramolecular Isomerism in Redox-Active Tetra- and Hexaruthenium Macrocycles. *Eur. J. Inorg. Chem.* **2020**, *2020*, 2816−2829.
(46) Fink, D.; Orth, N.; Linseis, M.; Ivanović-Burmazović, I.; Winter, R. F. Ring size matters: supramolecular isomerism in self-assembled redox-active tetra- and hexaruthenium macrocycles. *Chem. Commun.* **2020**, *56*, 1062−1065.
(47) Fink, D.; Orth, N.; Ebel, V.; Gogesch, F. S.; Staiger, A.; Linseis, M.; Ivanović-Burmazović, I.; Winter, R. F. Self-Assembled Redox-Active Tetraruthenium Macrocycles with Large Intracyclic Cavities. *Organometallics* **2020**, *39*, 1861−1880.
(48) Fink, D.; Linseis, M.; Winter, R. F. Constitutional Isomers of Macrocyclic Tetraruthenium Complexes with Vastly Different Spectroscopic and Electrochemical Properties. *Organometallics* **2018**, *37*, 1817−1820.
(49) Scheerer, S.; Linseis, M.; Wuttke, E.; Weickert, S.; Drescher, M.; Tröppner, O.; Ivanović-Burmazović, I.; Irmler, A.; Pauly, F.; Winter, R. F. Redox-Active Tetraruthenium Macrocycles Built from 1,4-Divinylphenylene-Bridged Diruthenium Complexes. *Chem.—Eur. J.* **2016**, *22*, 9574−9590.
(50) Fink, D.; Weibert, B.; Winter, R. F. Redox-active tetraruthenium metallacycles: reversible release of up to eight electrons resulting in strong electrochromism. *Chem. Commun.* **2016**, *52*, 6103−6106.
(51) Goeb, S.; Sallé, M. Electron-rich Coordination Receptors Based on Tetrathiafulvalene Derivatives: Controlling the Host-Guest Binding. *Acc. Chem. Res.* **2021**, *54*, 1043−1055.
(52) Huang, B.; Mao, L.; Shi, X.; Yang, H. B. Recent advances and perspectives on supramolecular radical cages. *Chem. Sci.* **2021**, *12*, 13648−13663.
(53) Fujita, M.; Sasaki, O.; Mitsuhashi, T.; Fujita, T.; Yazaki, J.; Yamaguchi, K.; Ogura, K. On the structure of transition-metal-linked molecular squares. *Chem. Commun.* **1996**, 1535−1536.
(54) Suzuki, K.; Kawano, M.; Fujita, M. Solvato-Controlled Assembly of Pd_3L_6 and Pd_4L_8 Coordination "Boxes". *Angew. Chem., Int. Ed.* **2007**, *46*, 2819−2822.
(55) Beves, J. E.; Blight, B. A.; Campbell, C. J.; Leigh, D. A.; McBurney, R. T. Strategies and tactics for the metal-directed synthesis of rotaxanes, knots, catenanes, and higher order links. *Angew. Chem.* **2011**, *50*, 9260−9327.
(56) Neogi, S.; Lorenz, Y.; Engeser, M.; Samanta, D.; Schmittel, M. Heteroleptic Metallosupramolecular Racks, Rectangles, and Trigonal Prisms: Stoichiometry-Controlled Reversible Interconversion. *Inorg. Chem.* **2013**, *52*, 6975−6984.
(57) Rancan, M.; Dolmella, A.; Seraglia, R.; Orlandi, S.; Quici, S.; Armelao, L. A templating guest sorts out a molecular triangle from a dimer−trimer constitutional dynamic library. *Chem. Commun.* **2012**, *48*, 3115−3117.
(58) Wang, W.; Wang, Y.-X.; Yang, H.-B. Supramolecular transformations within discrete coordination-driven supramolecular architectures. *Chem. Soc. Rev.* **2016**, *45*, 2656−2693.
(59) Garci, A.; Marti, S.; Schürch, S.; Therrien, B. Insight into the dynamic ligand exchange process involved in bipyridyl linked arene ruthenium metalla-rectangles. *RSC Adv.* **2014**, *4*, 8597−8604.
(60) Goswami, A.; Saha, S.; Biswas, P. K.; Schmittel, M. (Nano)-mechanical Motion Triggered by Metal Coordination: from Functional Devices to Networked Multicomponent Catalytic Machinery. *Chem. Rev.* **2020**, *120*, 125−199.
(61) Rotthowe, N.; Linseis, M.; Vogelsang, L.; Orth, N.; Ivanović-Burmazović, I.; Winter, R. F. A "Pretender" Croconate-Bridged Macrocyclic Tetraruthenium Complex: Sizable Redox Potential Splittings despite Electronically Insulated Divinylphenylene Diruthenium Entities. *Molecules* **2021**, *26*, 5232.
(62) Xia, H.; Jiang, X.; Lin, L.; Jiang, C.; Liao, G. Synthesis, crystal structures, and properties of inorganic-organic hybrid complexes constructed from copper(II) macrocyclic fragment. *Russ. J. Coord. Chem.* **2013**, *39*, 896−901.
(63) Feng, D.; Liu, T.-F.; Su, J.; Bosch, M.; Wei, Z.; Wan, W.; Yuan, D.; Chen, Y.-P.; Wang, X.; Wang, K.; Lian, X.; Gu, Z.-Y.; Park, J.; Zou, X.; Zhou, H.-C. Stable metal-organic frameworks containing single-molecule traps for enzyme encapsulation. *Nat. Commun.* **2015**, *6*, 5979.
(64) Choi, S.-H.; Bytheway, I.; Lin, Z.; Jia, G. Understanding the Preference for the Coplanarity of Alkenyl and Carbonyl Ligands in η^1-Alkenyl Transition-Metal Complexes: A Simple Molecular Orbital Approach and ab Initio Calculations. *Organometallics* **1998**, *17*, 3974−3980.
(65) Pfaff, U.; Hildebrandt, A.; Korb, M.; Oßwald, S.; Linseis, M.; Schreiter, K.; Spange, S.; Winter, R. F.; Lang, H. Electronically Strongly Coupled Divinylheterocyclic-Bridged Diruthenium Complexes. *Chem.—Eur. J.* **2016**, *22*, 783−801.

(66) Scheerer, S. Von Divinylarylen- und Tetraoxolenverbrückten Diruthenium-Komplexen zu Metallamakrozyklen. Doctoral Dissertation, University of Konstanz, 2017.
(67) Therrien, B. Arene Ruthenium Cages: Boxes Full of Surprises. *Eur. J. Inorg. Chem.* **2009**, *2009*, 2445−2453.
(68) Goeb, S.; Bivaud, S.; Dron, P. I.; Balandier, J.-Y.; Chas, M.; Sallé, M. A BPTTF-based self-assembled electron-donating triangle capable of C60 binding. *Chem. Commun.* **2012**, *48*, 3106−3108.
(69) Goeb, S.; Bivaud, S.; Croué, V.; Vajpayee, V.; Allain, M.; Sallé, M. A Self-Assembled Electro-Active M_8L_4 Cage Based on Tetrathiafulvalene Ligands. *Materials* **2014**, *7*, 611−622.
(70) Vajpayee, V.; Bivaud, S.; Goeb, S.; Croué, V.; Allain, M.; Popp, B. V.; Garci, A.; Therrien, B.; Sallé, M. Electron-Rich Arene−Ruthenium Metalla-architectures Incorporating Tetrapyridyl−Tetrathiafulvene Donor Moieties. *Organometallics* **2014**, *33*, 1651−1658.
(71) Krykun, S.; Allain, M.; Carre, V.; Aubriet, F.; Voitenko, Z.; Goeb, S.; Salle, M. A M2L2 redox-active metalla-macrocycle based on electron-rich 9-(1,3-dithiol-2-ylidene)fluorene. *Inorganics* **2018**, *6*, 44.
(72) Goeb, S.; Sallé, M. Electron-rich Coordination Receptors Based on Tetrathiafulvalene Derivatives: Controlling the Host−Guest Binding. *Acc. Chem. Res.* **2021**, *54*, 1043−1055.
(73) Kaim, W.; Schwederski, B.; Dogan, A.; Fiedler, J.; Kuehl, C. J.; Stang, P. J. Metalla-Supramolecular Rectangles as Electron Reservoirs for Multielectron Reduction and Oxidation. *Inorg. Chem.* **2002**, *41*, 4025−4028.
(74) Hartmann, H.; Berger, S.; Winter, R.; Fiedler, J.; Kaim, W. Reversible and Site-Specific Reduction of the Ligand Sides in a Molecular Rectangle with up to Eight Electrons. *Inorg. Chem.* **2000**, *39*, 4977−4980.
(75) Li, S.; Moorefield, C. N.; Wang, P.; Shreiner, C. D.; Newkome, G. R. Self-Assembly of Shape-Persistent Hexagonal Macrocycles with Trimeric Bis(terpyridine)−FeII Connectivity. *Eur. J. Org. Chem.* **2008**, *2008*, 3328−3334.
(76) Du, J.; Kodikara, M. S.; Moxey, G. J.; Morshedi, M.; Barlow, A.; Quintana, C.; Wang, G.; Stranger, R.; Zhang, C.; Cifuentes, M. P.; Humphrey, M. G. Quadratic and cubic hyperpolarizabilities of nitrophenyl/-naphthalenyl/-anthracenyl alkynyl complexes. *Dalton Trans.* **2018**, *47*, 4560−4571.
(77) Maurer, J.; Sarkar, B.; Schwederski, B.; Kaim, W.; Winter, R. F.; Záliš, S. Divinylphenylene-Bridged Diruthenium Complexes Bearing $Ru(CO)Cl(P^iPr_3)_2$ Entities. *Organometallics* **2006**, *25*, 3701−3712.
(78) Baranski, A. S.; Fawcett, W. R.; Gilbert, C. M. Use of Microelectrodes for the Rapid Determination of the Number of Electrons Involved in an Electrode Reaction. *Anal. Chem.* **1985**, *57*, 166−170.
(79) Matsumoto, M.; Swaddle, T. W. The Decamethylferrocene(+/0) Electrode Reaction in Organic Solvents at Variable Pressure and Temperature. *Inorg. Chem.* **2004**, *43*, 2724−2735.
(80) Krejčik, M.; Daněk, M.; Hartl, F. Simple construction of an infrared optically transparent thin-layer cell: Applications to the redox reactions of ferrocene, $Mn_2(CO)_{10}$ and $Mn(CO)_3$(3,5-di-t-butylcatecholate). *J. Electroanal. Chem. Interfacial Electrochem.* **1991**, *317*, 179−187.
(81) Robin, M. B.; Day, P. Mixed Valence Chemistry-A Survey and Classification. *Adv. Inorg. Chem. Radiochem.* **1968**, *10*, 247−422.
(82) Atwood, C. G.; Geiger, W. E. Investigation of Time-Dependent Delocalization and the Correlation of Carbonyl IR shifts with Delta $E_{1/2}$ values for Hydrocarbon Linked Class II and Class III Mixed-valent Complexes. *J. Am. Chem. Soc.* **2000**, *122*, 5477−5485.
(83) Stoll, M. E.; Lovelace, S. R.; Geiger, W. E.; Schimanke, H.; Hyla-Kryspin, I.; Gleiter, R. Transannular Effects in Dicobalta-Superphane Complexes on the Mixed-Valence Class II/ Class III Interface: Distinguishing between Spin and Charge Delocalization by Electrochemistry, Spectroscopy, and ab initio Calculations. *J. Am. Chem. Soc.* **1999**, *121*, 9343−9351.
(84) Pevny, F.; Di Piazza, E.; Norel, L.; Drescher, M.; Winter, R. F.; Rigaut, S. Fully Delocalized (Ethynyl)(vinyl)phenylene-Bridged Diruthenium Radical Complexes. *Organometallics* **2010**, *29*, 5912−5918.
(85) Das, R.; Linseis, M.; Schupp, S. M.; Schmidt-Mende, L.; Winter, R. F. Electron-Rich Diruthenium Complexes with π-Extended Alkenyl Ligands and Their F_4TCNQ Charge-Transfer Salts. *Chem.—Eur. J.* **2022**, *28*, No. e202104403.
(86) Anders, P.; Rapp, M.; Linseis, M.; Winter, R. Tetraruthenium Metallamacrocycles with Potentially Coordinating Appended Functionalities. *Inorganics* **2018**, *6*, 73.
(87) Abdel-Rahman, O. S.; Jan, M. T.; Oßwald, S.; Winter, R. F. Polyelectrochromism and electronic coupling in vinylruthenium-modified carbazoles. *J. Organomet. Chem.* **2017**, *849−850*, 98−116.
(88) Wuttke, E.; Hervault, Y.-M.; Polit, W.; Linseis, M.; Erler, P.; Rigaut, S.; Winter, R. F. Divinylphenylene- and Ethynylvinylphenylene-Bridged Mono-, Di-, and Triruthenium Complexes for Covalent Binding to Gold Electrodes. *Organometallics* **2014**, *33*, 4672−4686.
(89) Connelly, N. G.; Geiger, W. E. Chemical Redox Agents for Organometallic Chemistry. *Chem. Rev.* **1996**, *96*, 877−910.
(90) Croué, V.; Goeb, S.; Szalóki, G.; Allain, M.; Sallé, M. Reversible Guest Uptake/Release by Redox-Controlled Assembly/Disassembly of a Coordination Cage. *Angew. Chem.* **2016**, *55*, 1746−1750.
(91) Szalóki, G.; Krykun, S.; Croué, V.; Allain, M.; Morille, Y.; Aubriet, F.; Carré, V.; Voitenko, Z.; Goeb, S.; Sallé, M. Redox-Driven Transformation of a Discrete Molecular Cage into an Infinite 3D Coordination Polymer. *Chem.—Eur. J.* **2018**, *24*, 11273−11277.
(92) Scheerer, S.; Rotthowe, N.; Abdel-Rahman, O. S.; He, X.; Rigaut, S.; Kvapilová, H.; Záliš, S.; Winter, R. F. Vinyl ruthenium-modified biphenyl and 2,2′-bipyridines. *Inorg. Chem.* **2015**, *54*, 3387−3402.
(93) Hu, P.; Li, H.; Li, Y.; Jiang, H.; Kloc, C. Single-crystal growth, structures, charge transfer and transport properties of anthracene-F_4TCNQ and tetracene-F_4TCNQ charge-transfer compounds. *Cryst. Eng. Commun.* **2017**, *19*, 618−624.
(94) Hu, P.; Du, K.; Wei, F.; Jiang, H.; Kloc, C. Crystal Growth, HOMO−LUMO Engineering, and Charge Transfer Degree in Perylene-F_xTCNQ (x = 1, 2, 4) Organic Charge Transfer Binary Compounds. *Cryst. Growth Des.* **2016**, *16*, 3019−3027.
(95) Mahns, B.; Kataeva, O.; Islamov, D.; Hampel, S.; Steckel, F.; Hess, C.; Knupfer, M.; Büchner, B.; Himcinschi, C.; Hahn, T.; Renger, R.; Kortus, J. Crystal Growth, Structure, and Transport Properties of the Charge-Transfer Salt Picene/2,3,5,6-Tetrafluoro-7,7,8,8-tetracyanoquinodimethane. *Cryst. Growth Des.* **2014**, *14*, 1338−1346.
(96) Untilova, V.; Zeng, H.; Durand, P.; Herrmann, L.; Leclerc, N.; Brinkmann, M. Intercalation and Ordering of F_6TCNNQ and F_4TCNQ Dopants in Regioregular Poly(3-hexylthiophene) Crystals: Impact on Anisotropic Thermoelectric Properties of Oriented Thin Films. *Macromolecules* **2021**, *54*, 6073−6084.
(97) Zhu, L.; Geng, H.; Yi, Y.; Wei, Z. Charge transport in organic donor-acceptor mixed-stack crystals: the role of nonlocal electron-phonon couplings. *Phys. Chem. Chem. Phys.* **2017**, *19*, 4418−4425.
(98) Endo, T.; Akutagawa, T.; Kajiwara, T.; Kakiuchi, K.; Tatewaki, Y.; Noro, S.-i.; Nakamura, T. Langmuir−Blodgett Films of Charge-Transfer Complexes: Ethylenedithio-Substituted Amphiphilic Bis-TTF Macrocycle and F_4TCNQ or Br_2TCNQ. *Bull. Chem. Soc. Jpn.* **2009**, *82*, 968−974.
(99) Morherr, A.; Witt, S.; Chernenkaya, A.; Bäcker, J.-P.; Schönhense, G.; Bolte, M.; Krellner, C. Crystal growth of new charge-transfer salts based on π-conjugated donor molecules. *Phys. Rev. B* **2016**, *496*, 98−105.
(100) Sutton, A. L.; Abrahams, B. F.; D'Alessandro, D. M.; Hudson, T. A.; Robson, R.; Usov, P. M. Structural and optical investigations of charge transfer complexes involving the radical anions of TCNQ and F_4TCNQ. *CrystEngComm* **2016**, *18*, 8906−8914.
(101) Valencia, A. M.; Cocchi, C. Electronic and Optical Properties of Oligothiophene-F_4TCNQ Charge-Transfer Complexes: The Role of the Donor Conjugation Length. *J. Phys. Chem. C* **2019**, *123*, 9617−9623.
(102) Cochran, J. E.; Junk, M. J. N.; Glaudell, A. M.; Miller, P. L.; Cowart, J. S.; Toney, M. F.; Hawker, C. J.; Chmelka, B. F.; Chabinyc, M. L. Molecular Interactions and Ordering in Electrically Doped Polymers: Blends of PBTTT and F_4TCNQ. *Macromolecules* **2014**, *47*, 6836−6846.

(103) Rudloff, M.; Ackermann, K.; Huth, M.; Jeschke, H. O.; Tomic, M.; Valentí, R.; Wolfram, B.; Bröring, M.; Bolte, M.; Chercka, D.; Baumgarten, M.; Müllen, K. Charge transfer tuning by chemical substitution and uniaxial pressure in the organic complex tetramethoxypyrene-tetracyanoquinodimethane. *Phys. Chem. Chem. Phys.* **2015**, *17*, 4118−4126.
(104) Das, R.; Linseis, M.; Senft, L.; Ivanović-Burmazović, I.; Winter, R. F. Tetraruthenium Macrocycles With Laterally Extended Bis(alkenyl)quinoxaline Ligands and Their F_4TCNQ^- Salts. *Inorganics* **2022**, *10*, 82.
(105) Gerson, F.; Heckendorn, R.; Cowan, D. O.; Kini, A. M.; Maxfield, M. Radical anions and radical trianions of tetracyanoarenoquinodimethanes. An ESR and ENDOR study. *J. Am. Chem. Soc.* **1983**, *105*, 7017−7023.
(106) O'Kane, S. A.; Clérac, R.; Zhao, H.; Ouyang, X.; Galán-Mascarós, J. R.; Heintz, R.; Dunbar, K. R. New Crystalline Polymers of Ag(TCNQ) and Ag($TCNQF_4$): Structures and Magnetic Properties. *J. Solid State Chem.* **2000**, *152*, 159−173.
(107) Stoll, S.; Schweiger, A. EasySpin, a comprehensive software package for spectral simulation and analysis in EPR. *J. Magn. Reson.* **2006**, *178*, 42−55.
(108) Boduszek, B.; Shine, H. J. Preparation of Solid Thianthrene Cation Radical Tetrafluoroborate. *J. Org. Chem.* **1988**, *53*, 5142−5143.
(109) Dolomanov, O. V.; Bourhis, L. J.; Gildea, R. J.; Howard, J. A. K.; Puschmann, H. OLEX2: a complete structure solution, refinement and analysis program. *J. Appl. Cryst.* **2009**, *42*, 339−341.
(110) Sheldrick, G. M. Crystal structure refinement with SHELXL. *Acta Crystallogr., Sect. C: Struct. Chem.* **2015**, *71*, 3−8.
(111) Macrae, C. F.; Bruno, I. J.; Chisholm, J. A.; Edgington, P. R.; McCabe, P.; Pidcock, E.; Rodriguez-Monge, L.; Taylor, R.; van de Streek, J.; Wood, P. A. Mercury CSD 2.0− new features for the visualization and investigation of crystal structures. *J. Appl. Cryst.* **2008**, *41*, 466−470.
(112) Schrödinger, L.; DeLano, W. PyMOL. 2020, available at: http://www.pymol.org/pymol (accessed Nov 15, 2021).